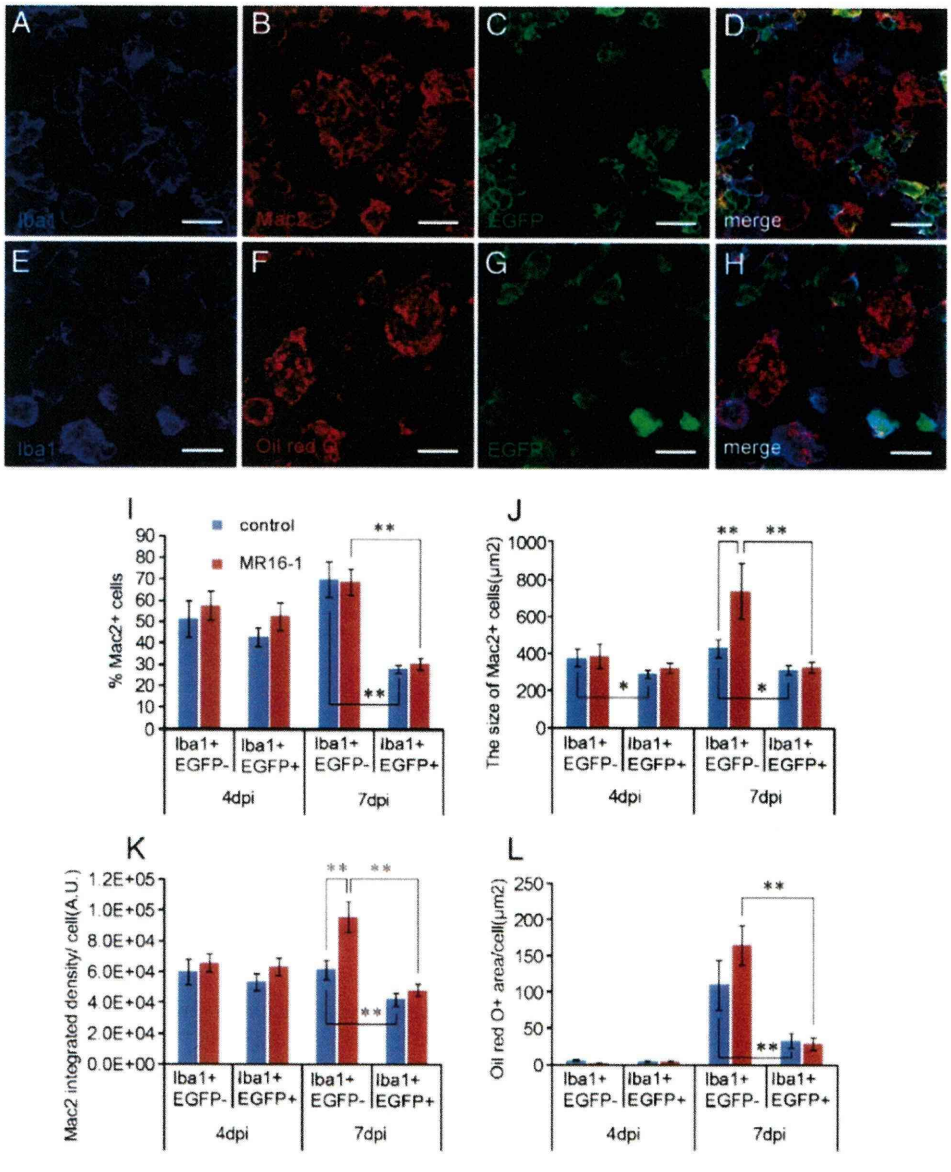

Fig. 5. Microglia have higher phagocytic activity against myelin debris than hematogenous macrophages. A–D: Mac2 expression was observed in the cells at the lesion epicenter. A portion of the macrophages/microglia expressed Mac2 in their cytoplasm. E–H: Oil red O$^+$ particles were observed in the cell body of macrophages/microglia at the lesion epicenter. I: The cytoplasmic expression of Mac2 was greater in Iba1$^+$EGFP$^-$ resident microglia than in Iba1$^+$EGFP$^+$ hematogenous macrophages. J, K: The average size (J) and Mac2-integrated density (K) at 7 dpi of each Iba1$^+$EGFP$^-$ resident microglial cell were significantly greater than those of Iba1$^+$EGFP$^+$ hematogenous macrophages, and were increased by MR16-1 treatment. The intracellular Oil red O-stained area was significantly greater in the Iba1$^+$EGFP$^-$ resident microglia than in the Iba1$^+$EGFP$^+$ hematogenous macrophages, and this tendency was increased at 7 dpi by MR16-1 treatment (L). Values are means ± SEM. *P<0.05. **P<0.01. Scale bars = 20 μm in A–H.

Nogo-A, which showed reduced injury and deposition of debris, support this idea. This series of immune responses takes place over a long time, which is consistent with the effects of MR16-1 treatment appearing only at the late phase.

However, despite the marked improvement in the inflammatory response obtained with MR16-1 treatment, skepticism about the therapeutic effects of IL-6 signal inhibition remains, because several studies have shown that IL-6 signaling has neuroprotective functions after CNS trauma. For example, Penkowa et al. showed that the overexpression of IL-6 results in decreased oxidative stress and apoptosis, leading to faster tissue repair after brain injury (Penkowa et al., 2003), and IL-6-deficient mice show a slower rate of recovery and healing after brain injury than wild-type mice (Swartz et al., 2001).

Although our results may seem to conflict with these reports, we believe that the apparent discrepancies are owing to the context-dependent pleiotropic actions of IL-6. Our present data revealed that the therapeutic effect of MR16-1 was achieved by inhibiting the excessive infiltration of hematogenous macrophages through the damaged BSCB, during the acute phase of SCI. This idea is corroborated by previous reports demonstrating that the overexpression of IL-6 family cytokines during the acute phase of SCI significantly increases inflammatory cell accumulation, resulting in greater damage (Kerr and Patterson, 2004; Lacroix et al., 2002). On the other hand, IL-6 can enhance spinal cord repair by modifying the migration of reactive astrocytes (Okada et al., 2006) or enhancing axonal re-growth (Miao et al., 2006), and IL-6's temporary inhibition may have little effect on these functions, because astrocyte migration and axonal re-growth are rather long-term processes. Although numerous studies have shown that the recruitment of inflammatory cells aggravates secondary injury after SCI (Ghirnikar et al., 2001; Hausmann, 2003;

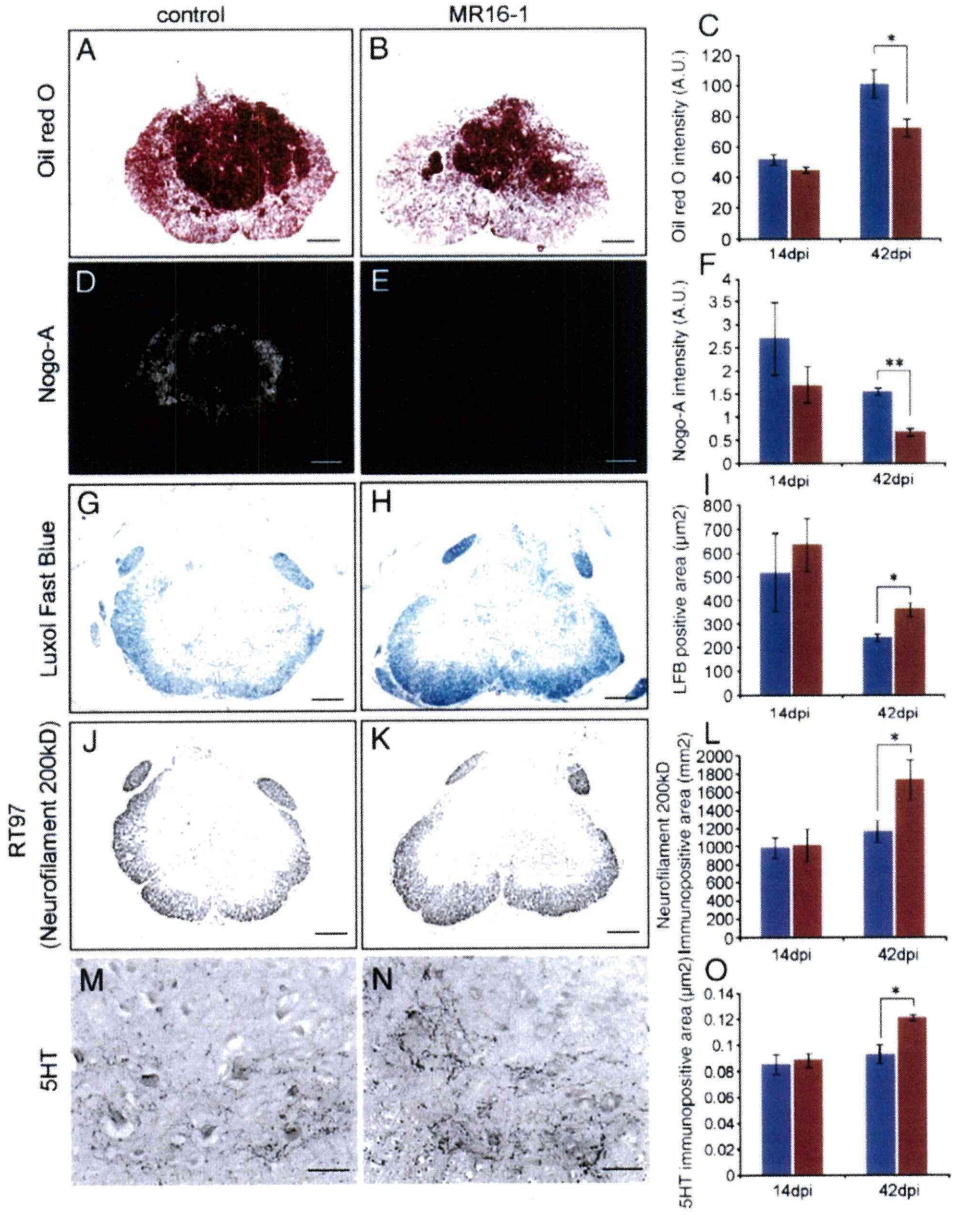

Fig. 6. MR16-1 treatment improves repair of the spinal cord. A–C: MR16-1 treatment improved the clearance of myelin debris, as seen by a significant reduction in the Oil red O-stained area. D–F: The deposition of Nogo-A was decreased in the MR16-1-treated group. G–I: The area of Luxol Fast Blue-stained tissue, which represents spared myelin sheath, was significantly increased by the MR16-1 treatment. J–L: RT-97^{+} (Neurofilament 200kD) fibers at the lesion epicenter were significantly increased in the MR16-1-treated animals at 42 dpi. M–O: 5HT-positive fibers at the ventral horn. 5HT-immunostaining of the area 2 mm caudal to the lesion revealed a significant increase in 5HT^{+} fibers at 42 dpi by the MR16-1-treatment. *$P<0.05$. Scale bars = 200 μm in A, B, D, E, G, H; 50 μm in J, K.

Saville et al., 2004), inflammation itself is important for spinal cord repair (Donnelly and Popovich, 2008), and excessive suppression of the inflammatory response can be detrimental. In the present study, we showed that anti-IL-6-receptor antibody treatment at the acute stage of injury switches the main subpopulation of inflammatory cells from hematogenous macrophages to microglia, which does not simply suppress inflammation: rather, it changes the characteristics of the post-traumatic inflammation to promote spinal cord repair.

Given that a humanized antibody for the human IL-6 receptor (MRA; tocilizumab) is already in clinical use (Choy et al., 2002; Nishimoto et al., 2000; Sato et al., 1993), the present data support the potential application of the anti-IL-6-receptor antibody for the treatment of SCI. However, in most clinical situations, it is not possible to administer an antibody immediately after SCI. Further investigation to determine the therapeutic time window will be needed before this treatment can be tried clinically. Nevertheless, these findings shed light on IL-6's role in the pathology of SCI, and suggest a new approach for SCI treatment, in which the characteristics of inflammation are adjusted to support spinal cord repair, by modifying the cytokine-mediated cellular response.

Author contributions

M.M., M.N., Y.T., M.L. and H.O. designed the research; M.M., O.Y., A. I., T.I., F.RM. and O.T. performed the in vivo experiments; S.M. and Y.M. generated the chimeric mice; Y.O. supplied the anti-IL-6 receptor antibody and analyzed the antibody results; M.M., M.N., S.O., F.RM. and H.K. analyzed the data; M.M., M.N. and H.O. wrote the paper; M.N. and H.O. supervised all the experiments.

Acknowledgments

This work was supported by grants from the Project for the Realization of Regenerative Medicine from the Ministry of Education, Culture, Sports, Science and Technology (MEXT), Japan to H.O.; the General Insurance Association of Japan to M.N., A.I. and Y.T.; and a Grant-in-Aid for the Global COE Program from MEXT to Keio University. This work was also supported by grants from the Grant of Orthopaedics and Traumatology Foundation, Inc. No. 0178 to A.I. We are grateful to Professor Claude Bernard at Monash University for his critical reading of the manuscript.

Appendix A. Supplementary data

Supplementary data associated with this article can be found, in the online version, at doi:10.1016/j.expneurol.2010.04.020.

References

Babcock, A.A., Kuziel, W.A., Rivest, S., Owens, T., 2003. Chemokine expression by glial cells directs leukocytes to sites of axonal injury in the CNS. J. Neurosci. 23, 7922–7930.

Bomstein, Y., Marder, J.B., Vitner, K., Smirnov, I., Lisaey, G., Butovsky, O., Fulga, V., Yoles, E., 2003. Features of skin-coincubated macrophages that promote recovery from spinal cord injury. J. Neuroimmunol. 142, 10–16.

Bregman, B.S., Kunkel-Bagden, E., Schnell, L., Dai, H.N., Gao, D., Schwab, M.E., 1995. Recovery from spinal cord injury mediated by antibodies to neurite growth inhibitors. Nature 378, 498–501.

Cafferty, W.B., Gardiner, N.J., Das, P., Qiu, J., McMahon, S.B., Thompson, S.W., 2004. Conditioning injury-induced spinal axon regeneration fails in interleukin-6 knock-out mice. J. Neurosci. 24, 4432–4443.

Choy, E.H., Isenberg, D.A., Garrood, T., Farrow, S., Ioannou, Y., Bird, H., Cheung, N., Williams, B., Hazleman, B., Price, R., Yoshizaki, K., Nishimoto, N., Kishimoto, T., Panayi, G.S., 2002. Therapeutic benefit of blocking interleukin-6 activity with an anti-interleukin-6 receptor monoclonal antibody in rheumatoid arthritis: a randomized, double-blind, placebo-controlled, dose-escalation trial. Arthritis Rheum. 46, 3143–3150.

Donnelly, D.J., Popovich, P.G., 2008. Inflammation and its role in neuroprotection, axonal regeneration and functional recovery after spinal cord injury. Exp. Neurol. 209, 378–388.

Gensel, J.C., Nakamura, S., Guan, Z., van Rooijen, N., Ankeny, D.P., Popovich, P.G., 2009. Macrophages promote axon regeneration with concurrent neurotoxicity. J. Neurosci. 29, 3956–3968.

Ghirnikar, R.S., Lee, Y.L., Li, J.D., Eng, L.F., 1998. Chemokine inhibition in rat stab wound brain injury using antisense oligodeoxynucleotides. Neurosci. Lett. 247, 21–24.

Ghirnikar, R.S., Lee, Y.L., Eng, L.F., 2001. Chemokine antagonist infusion promotes axonal sparing after spinal cord contusion injury in rat. J. Neurosci. Res. 64, 582–589.

Giulian, D., Ingeman, J.E., 1988. Colony-stimulating factors as promoters of ameboid microglia. J. Neurosci. 8, 4707–4717.

Glass, W.G., Liu, M.T., Kuziel, W.A., Lane, T.E., 2001. Reduced macrophage infiltration and demyelination in mice lacking the chemokine receptor CCR5 following infection with a neurotropic coronavirus. Virology 288, 8–17.

Gris, D., Marsh, D.R., Oatway, M.A., Chen, Y., Hamilton, E.F., Dekaban, G.A., Weaver, L.C., 2004. Transient blockade of the CD11d/CD18 integrin reduces secondary damage after spinal cord injury, improving sensory, autonomic, and motor function. J. Neurosci. 24, 4043–4051.

Hashimoto, M., Nitta, A., Fukumitsu, H., Nomoto, H., Shen, L., Furukawa, S., 2005. Involvement of glial cell line-derived neurotrophic factor in activation processes of rodent macrophages. J. Neurosci. Res. 79, 476–487.

Hausmann, O.N., 2003. Post-traumatic inflammation following spinal cord injury. Spinal Cord 41, 369–378.

Horn, K.P., Busch, S.A., Hawthorne, A.L., van Rooijen, N., Silver, J., 2008. Another barrier to regeneration in the CNS: activated macrophages induce extensive retraction of dystrophic axons through direct physical interactions. J. Neurosci. 28, 9330–9341.

Hurst, S.M., Wilkinson, T.S., McLoughlin, R.M., Jones, S., Horiuchi, S., Yamamoto, N., Rose-John, S., Fuller, G.M., Topley, N., Jones, S.A., 2001. Il-6 and its soluble receptor orchestrate a temporal switch in the pattern of leukocyte recruitment seen during acute inflammation. Immunity 14, 705–714.

Kawamoto, S., Niwa, H., Tashiro, F., Sano, S., Kondoh, G., Takeda, J., Tabayashi, K., Miyazaki, J., 2000. A novel reporter mouse strain that expresses enhanced green fluorescent protein upon Cre-mediated recombination. FEBS Lett. 470, 263–268.

Kerr, B.J., Patterson, P.H., 2004. Potent pro-inflammatory actions of leukemia inhibitory factor in the spinal cord of the adult mouse. Exp. Neurol. 188, 391–407.

Klusman, I., Schwab, M.E., 1997. Effects of pro-inflammatory cytokines in experimental spinal cord injury. Brain Res. 762, 173–184.

Koide, Y., Morikawa, S., Mabuchi, Y., Muguruma, Y., Hiratsu, E., Hasegawa, K., Kobayashi, M., Ando, K., Kinjo, K., Okano, H., Matsuzaki, Y., 2007. Two distinct stem cell lineages in murine bone marrow. Stem Cells 25, 1213–1221.

Koopman, R., Schaart, G., Hesselink, M.K., 2001. Optimisation of oil red O staining permits combination with immunofluorescence and automated quantification of lipids. Histochem. Cell Biol. 116, 63–68.

Lacroix, S., Chang, L., Rose-John, S., Tuszynski, M.H., 2002. Delivery of hyper-interleukin-6 to the injured spinal cord increases neutrophil and macrophage infiltration and inhibits axonal growth. J. Comp. Neurol. 454, 213–228.

Lalancette-Hebert, M., Gowing, G., Simard, A., Weng, Y.C., Kriz, J., 2007. Selective ablation of proliferating microglial cells exacerbates ischemic injury in the brain. J. Neurosci. 27, 2596–2605.

Lambertsen, K.L., Clausen, B.H., Babcock, A.A., Gregersen, R., Fenger, C., Nielsen, H.H., Haugaard, L.S., Wirenfeldt, M., Nielsen, M., Dagnaes-Hansen, F., Bluethmann, H., Faergeman, N.J., Meldgaard, M., Deierborg, T., Finsen, B., 2009. Microglia protect neurons against ischemia by synthesis of tumor necrosis factor. J. Neurosci. 29, 1319–1330.

Lee, S.C., Liu, W., Brosnan, C.F., Dickson, D.W., 1994. GM-CSF promotes proliferation of human fetal and adult microglia in primary cultures. Glia 12, 309–318.

Liu, M.T., Keirstead, H.S., Lane, T.E., 2001. Neutralization of the chemokine CXCL10 reduces inflammatory cell invasion and demyelination and improves neurological function in a viral model of multiple sclerosis. J. Immunol. 167, 4091–4097.

Matsumura, M., Banba, N., Motohashi, S., Hattori, Y., 1999. Interleukin-6 and transforming growth factor-beta regulate the expression of monocyte chemoattractant protein-1 and colony-stimulating factors in human thyroid follicular cells. Life Sci. 65, PL129–PL135.

Matsuzaki, Y., Kinjo, K., Mulligan, R.C., Okano, H., 2004. Unexpectedly efficient homing capacity of purified murine hematopoietic stem cells. Immunity 20, 87–93.

McTigue, D.M., Popovich, P.G., Morgan, T.E., Stokes, B.T., 2000. Localization of transforming growth factor-beta1 and receptor mRNA after experimental spinal cord injury. Exp. Neurol. 163, 220–230.

Merkler, D., Metz, G.A., Raineteau, O., Dietz, V., Schwab, M.E., Fouad, K., 2001. Locomotor recovery in spinal cord-injured rats treated with an antibody neutralizing the myelin-associated neurite growth inhibitor Nogo-A. J. Neurosci. 21, 3665–3673.

Miao, T., Wu, D., Zhang, Y., Bo, X., Subang, M.C., Wang, P., Richardson, P.M., 2006. Suppressor of cytokine signaling-3 suppresses the ability of activated signal transducer and activator of transcription-3 to stimulate neurite growth in rat primary sensory neurons. J. Neurosci. 26, 9512–9519.

Mildenberger, M., Beach, T.G., McGeer, E.G., Ludgate, C.M., 1990. An animal model of prophylactic cranial irradiation: histologic effects at acute, early and delayed stages. Int. J. Radiat. Oncol. Biol. Phys. 18, 1051–1060.

Nesic, O., Xu, G.Y., McAdoo, D., High, K.W., Hulsebosch, C., Perez-Pol, R., 2001. IL-1 receptor antagonist prevents apoptosis and caspase-3 activation after spinal cord injury. J. Neurotrauma 18, 947–956.

Nishimoto, N., Sasai, M., Shima, Y., Nakagawa, M., Matsumoto, T., Shirai, T., Kishimoto, T., Yoshizaki, K., 2000. Improvement in Castleman's disease by humanized anti-interleukin-6 receptor antibody therapy. Blood 95, 56–61.

Okada, S., Nakamura, M., Mikami, Y., Shimazaki, T., Mihara, M., Ohsugi, Y., Iwamoto, Y., Yoshizaki, K., Kishimoto, T., Toyama, Y., Okano, H., 2004. Blockade of interleukin-6 receptor suppresses reactive astrogliosis and ameliorates functional recovery in experimental spinal cord injury. J. Neurosci. Res. 76, 265–276.

Okada, S., Nakamura, M., Katoh, H., Miyao, T., Shimazaki, T., Ishii, K., Yamane, J., Yoshimura, A., Iwamoto, Y., Toyama, Y., Okano, H., 2006. Conditional ablation of Stat3 or Socs3 discloses a dual role for reactive astrocytes after spinal cord injury. Nat. Med. 12, 829–834.

Okazaki, M., Yamada, Y., Nishimoto, N., Yoshizaki, K., Mihara, M., 2002. Characterization of anti-mouse interleukin-6 receptor antibody. Immunol. Lett. 84, 231–240.

Penkowa, M., Giralt, M., Lago, N., Camats, J., Carrasco, J., Hernandez, J., Molinero, A., Campbell, I.L., Hidalgo, J., 2003. Astrocyte-targeted expression of IL-6 protects the CNS against a focal brain injury. Exp. Neurol. 181, 130–148.

Ponomarev, E.D., Maresz, K., Tan, Y., Dittel, B.N., 2007. CNS-derived interleukin-4 is essential for the regulation of autoimmune inflammation and induces a state of alternative activation in microglial cells. J. Neurosci. 27, 10714–10721.

Popovich, P.G., Guan, Z., Wei, P., Huitinga, I., van Rooijen, N., Stokes, B.T., 1999. Depletion of hematogenous macrophages promotes partial hindlimb recovery and neuroanatomical repair after experimental spinal cord injury. Exp. Neurol. 158, 351–365.

Popovich, P.G., Guan, Z., McGaughy, V., Fisher, L., Hickey, W.F., Basso, D.M., 2002. The neuropathological and behavioral consequences of intraspinal microglial/macrophage activation. J. Neuropathol. Exp. Neurol. 61, 623–633.

Rapalino, O., Lazarov-Spiegler, O., Agranov, E., Velan, G.J., Yoles, E., Fraidakis, M., Solomon, A., Gepstein, R., Katz, A., Belkin, M., Hadani, M., Schwartz, M., 1998. Implantation of stimulated homologous macrophages results in partial recovery of paraplegic rats. Nat. Med. 4, 814–821.

Rinner, W.A., Bauer, J., Schmidts, M., Lassmann, H., Hickey, W.F., 1995. Resident microglia and hematogenous macrophages as phagocytes in adoptively transferred experimental autoimmune encephalomyelitis: an investigation using rat radiation bone marrow chimeras. Glia 14, 257–266.

Romano, M., Sironi, M., Toniatti, C., Polentarutti, N., Fruscella, P., Ghezzi, P., Faggioni, R., Luini, W., van Hinsbergh, V., Sozzani, S., Bussolino, F., Poli, V., Ciliberto, G., Mantovani, A., 1997. Role of IL-6 and its soluble receptor in induction of chemokines and leukocyte recruitment. Immunity 6, 315–325.

Rotshenker, S., Reichert, F., Gitik, M., Haklai, R., Elad-Sfadia, G., Kloog, Y., 2008. Galectin-3/MAC-2, Ras and PI3K activate complement receptor-3 and scavenger receptor-AI/II mediated myelin phagocytosis in microglia. Glia 56, 1607–1613.

Sato, K., Tsuchiya, M., Saldanha, J., Koishihara, Y., Ohsugi, Y., Kishimoto, T., Bendig, M.M., 1993. Reshaping a human antibody to inhibit the interleukin 6-dependent tumor cell growth. Cancer Res. 53, 851–856.

Saville, L.R., Pospisil, C.H., Mawhinney, L.A., Bao, F., Simedrea, F.C., Peters, A.A., O'Connell, P.J., Weaver, L.C., Dekaban, G.A., 2004. A monoclonal antibody to CD11d reduces the inflammatory infiltrate into the injured spinal cord: a potential neuroprotective treatment. J. Neuroimmunol. 156, 42–57.

Schilling, M., Besselmann, M., Muller, M., Strecker, J.K., Ringelstein, E.B., Kiefer, R., 2005. Predominant phagocytic activity of resident microglia over hematogenous macrophages following transient focal cerebral ischemia: an investigation using green fluorescent protein transgenic bone marrow chimeric mice. Exp. Neurol. 196, 290–297.

Schwartz, M., Lazarov-Spiegler, O., Rapalino, O., Agranov, I., Velan, G., Hadani, M., 1999. Potential repair of rat spinal cord injuries using stimulated homologous macrophages. Neurosurgery 44, 1041–1045 discussion 1045-1046.

Sedgwick, J.D., Schwender, S., Imrich, H., Dorries, R., Butcher, G.W., ter Meulen, V., 1991. Isolation and direct characterization of resident microglial cells from the normal and inflamed central nervous system. Proc. Natl. Acad. Sci. U. S. A. 88, 7438–7442.

Sharma, H.S., Winkler, T., Stalberg, E., Gordh, T., Alm, P., Westman, J., 2003. Topical application of TNF-alpha antiserum attenuates spinal cord trauma induced edema formation, microvascular permeability disturbances and cell injury in the rat. Acta Neurochir. Suppl. 86, 407–413.

Steinmetz, M.P., Horn, K.P., Tom, V.J., Miller, J.H., Busch, S.A., Nair, D., Silver, D.J., Silver, J., 2005. Chronic enhancement of the intrinsic growth capacity of sensory neurons combined with the degradation of inhibitory proteoglycans allows functional regeneration of sensory axons through the dorsal root entry zone in the mammalian spinal cord. J. Neurosci. 25, 8066–8076.

Swartz, K.R., Liu, F., Sewell, D., Schochet, T., Campbell, I., Sandor, M., Fabry, Z., 2001. Interleukin-6 promotes post-traumatic healing in the central nervous system. Brain Res. 896, 86–95.

Tamura, T., Udagawa, N., Takahashi, N., Miyaura, C., Tanaka, S., Yamada, Y., Koishihara, Y., Ohsugi, Y., Kumaki, K., Taga, T., et al., 1993. Soluble interleukin-6 receptor triggers osteoclast formation by interleukin 6. Proc. Natl. Acad. Sci. U. S. A. 90, 11924–11928.

Tuna, M., Polat, S., Erman, T., Ildan, F., Gocer, A.I., Tuna, N., Tamer, L., Kaya, M., Cetinalp, E., 2001. Effect of anti-rat interleukin-6 antibody after spinal cord injury in the rat: inducible nitric oxide synthase expression, sodium- and potassium-activated, magnesium-dependent adenosine-5′-triphosphatase and superoxide dismutase activation, and ultrastructural changes. J. Neurosurg. 95, 64–73.

Turrin, N.P., Plante, M.M., Lessard, M., Rivest, S., 2007. Irradiation does not compromise or exacerbate the innate immune response in the brains of mice that were transplanted with bone marrow stem cells. Stem Cells 25, 3165–3172.

Van Wagoner, N.J., Benveniste, E.N., 1999. Interleukin-6 expression and regulation in astrocytes. J. Neuroimmunol. 100, 124–139.

Therapeutic potential of appropriately evaluated safe-induced pluripotent stem cells for spinal cord injury

Osahiko Tsuji[a,b,1], Kyoko Miura[a,c,1], Yohei Okada[a,d], Kanehiro Fujiyoshi[a,b], Masahiko Mukaino[a,e], Narihito Nagoshi[a,b,f], Kazuya Kitamura[a,b], Gentaro Kumagai[a,g], Makoto Nishino[a], Shuta Tomisato[a], Hisanobu Higashi[a], Toshihiro Nagai[h], Hiroyuki Katoh[a,b,f], Kazuhisa Kohda[a], Yumi Matsuzaki[a], Michisuke Yuzaki[a], Eiji Ikeda[i,j], Yoshiaki Toyama[b], Masaya Nakamura[b,2], Shinya Yamanaka[c], and Hideyuki Okano[a,2]

Departments of [a]Physiology and [b]Orthopedic Surgery, School of Medicine, Keio University, Shinjuku, Tokyo 160-8582, Japan; [c]Center for Induced Pluripotent Stem Cell Research and Application, Kyoto University, Kyoto 606-8507, Japan; [d]Kanrinmaru-Project and Departments of [e]Rehabilitation Medicine, [h]Electron Microscope Laboratory, and [i]Pathology, School of Medicine, Keio University, Tokyo 160-8582, Japan; [f]Department of Orthopedic Surgery, National Hospital Organization, Murayama Medical Center, Tokyo 208-0011, Japan; [g]Department of Orthopedic Surgery, Graduate School of Medicine, Hirosaki University, Aomori 036-8560, Japan; and [j]Department of Pathology, Graduate School of Medicine, Yamaguchi University, Yamaguchi 755-8505, Japan

Edited by Fred Gage, Salk Institute, San Diego, CA, and approved June 3, 2010 (received for review September 3, 2009)

Various types of induced pluripotent stem (iPS) cells have been established by different methods, and each type exhibits different biological properties. Before iPS cell-based clinical applications can be initiated, detailed evaluations of the cells, including their differentiation potentials and tumorigenic activities in different contexts, should be investigated to establish their safety and effectiveness for cell transplantation therapies. Here we show the directed neural differentiation of murine iPS cells and examine their therapeutic potential in a mouse spinal cord injury (SCI) model. "Safe" iPS-derived neurospheres, which had been pre-evaluated as nontumorigenic by their transplantation into nonobese diabetic/severe combined immunodeficiency (NOD/SCID) mouse brain, produced electrophysiologically functional neurons, astrocytes, and oligodendrocytes in vitro. Furthermore, when the safe iPS-derived neurospheres were transplanted into the spinal cord 9 d after contusive injury, they differentiated into all three neural lineages without forming teratomas or other tumors. They also participated in remyelination and induced the axonal regrowth of host 5HT$^+$ serotonergic fibers, promoting locomotor function recovery. However, the transplantation of iPS-derived neurospheres pre-evaluated as "unsafe" showed robust teratoma formation and sudden locomotor functional loss after functional recovery in the SCI model. These findings suggest that pre-evaluated safe iPS clone-derived neural stem/progenitor cells may be a promising cell source for transplantation therapy for SCI.

neural stem/progenitor cell | cell transplantation | regenerative medicine | remyelination | axonal regrowth

Given their ability to generate all types of neural cells, neural stem/progenitor cells (NS/PCs) are a promising source for cell replacement therapy for various intractable CNS disorders (reviewed in refs. 1–6). Notably, ES cells have great developmental plasticity and can be induced to become NS/PCs with specific differentiation potentials (7–11), making them a major candidate for cell replacement therapies for CNS disorders (12–16). The clinical use of ES cells is complicated, however, by ethical and immunological concerns, both of which might be overcome by using pluripotent stem cells derived directly from a patient's own somatic cells (17).

We recently reported the establishment of induced pluripotent stem (iPS) cells from mouse fibroblasts by the retroviral introduction of four factors (*Oct3/4*, *Sox2*, *Klf4*, and *c-Myc*) with selection for *Fbxo15* expression (18) and *Nanog* expression (19, 20). Compared with *Fbxo15*-selected iPS cells, *Nanog*-selected iPS cells more closely resembled ES cells' gene-expression pattern and could contribute to germline-competent adult chimeras (19–21). More recently, we and others (22, 23) generated iPS cells without using *c-Myc* retroviruses, albeit with lower efficiency. The successful establishment of these iPS cell lines, along with initial reports showing efficacy in the therapeutic use of iPS cells in rodent models of sickle cell anemia (24) and Parkinson disease (25), led us to examine the use of iPS cells as a treatment for spinal cord injury (SCI).

A number of important issues need to be addressed before a clinical trial using iPS cells as a cell-therapy source for SCI is initiated. First, a detailed evaluation of iPS cells' potential to generate neural cells compared with ES cells is required. Second, iPS cells are likely to carry a higher risk of tumorigenicity than ES cells, due to the inappropriate reprogramming of these somatic cells, the activation of exogenous transcription factors, or other reasons (25–27). Thus, it is essential to confirm the safety of grafted iPS-derived NS/PCs. Finally, the effectiveness of iPS-derived NS/PC transplantation as a treatment for SCI must be evaluated.

In the previous study, we pre-evaluated iPS clones for safety by transplanting iPS-derived neurospheres into the NOD/SCID mouse brain (27). Here, we show that the transplantation of neurospheres derived from safe iPS cell clones into the injured spinal cord promoted functional recovery without any tumor formation. In contrast, the transplantation of neurospheres derived from unsafe iPS cells, showing robust teratoma formation in the NOD/SCID mouse brain, also resulted in initial functional recovery, but was later followed by teratoma formation and deterioration of locomotor function. These data suggest that the evaluation of in vitro differentiation and in vivo tumorigenicity are important for identifying safe iPS clones for cell therapy, and that the NS/PCs derived from iPS clones deemed safe by such pre-evaluation are a promising source for cell therapy for SCI.

Results

Pre-Evaluated Safe MEF-iPS Cells Exhibit ES-Like Neural Differentiation Potentials in Vitro. We previously reported the neural differentiation of 36 independent murine iPS cell clones (27). The results of this study led us to classify several iPS clones as safe or unsafe

Author contributions: O.T., K.M., M. Nakamura, S.Y., and H.O. designed research; O.T., K.M., Y.O., K.F., M.M., N.N., K. Kitamura, G.K., M. Nishino, S.T., H.H., T.N., H.K., E.I., and H.O. performed research; O.T. and K.M. contributed new reagents/analytic tools; O.T., K.M., Y.O., K.F., M.M., N.N., K. Kitamura, G.K., H.K., K. Kohda, Y.M., M.Y., E.I., Y.T., M. Nakamura, S.Y., and H.O. analyzed data; and O.T., K.M., Y.O., K.F., H.K., E.I., M. Nakamura, and H.O. wrote the paper.

The authors declare no conflict of interest.

This article is a PNAS Direct Submission.

[1]O.T. and K.M. contributed equally to this work.

[2]To whom correspondence may be addressed. E-mail: hidokano@sc.itc.keio.ac.jp or masa@sc.itc.keio.ac.jp.

This article contains supporting information online at www.pnas.org/lookup/suppl/doi:10.1073/pnas.0910106107/-/DCSupplemental.

clones, according to the teratoma-forming activity of the iPS-derived neurospheres after transplantation into the NOD/SCID mouse brain.

Here, we first performed a detailed examination of the neural differentiation potential of a safe iPS clone, 38C2, which was established from mouse embryonic fibroblasts (MEFs) by the introduction of four factors, including *c-Myc*, and by the selection for *Nanog* expression (19, 28), and compared them with mouse ES cells (EB3) (29, 30). 38C2 iPS cells and EB3 ES cells were induced into embryoid bodies (EBs) in medium containing a low concentration of retinoic acid, then dissociated and cultured in suspension in serum-free medium with FGF-2 for 7 or 8 d to form primary neurospheres (PNS) (38C2 iPS/EB3 ES-PNS) (29). These PNSs were dissociated and formed secondary neurospheres (38C2 iPS/EB3 ES-SNS) under the same conditions (Fig. 1*A*). To induce further differentiation, 38C2 iPS-SNSs were adherently cultured in the absence of FGF-2, resulting in the generation of Tuj1$^+$ neurons (4.9 ± 0.8%), GFAP$^+$ astrocytes (11.3 ± 1.2%), and CNPase$^+$ oligodendrocytes (3.7 ± 0.9%), as well as Nestin$^+$ neural progenitor cells (25.9 ± 6.5%; Fig. 1 *B* and *C*), suggesting that 38C2 iPS-SNS have similar differentiation potentials to EB3 ES-SNS. The 38C2 iPS-PNSs could also generate TH$^+$ catecholaminergic, 5HT$^+$ serotonergic, and GAD67$^+$ GABAergic neurons (Fig. S1). RT-PCR analysis of the expression of cell-type-specific markers in the progeny of the 38C2 iPS cells showed drastic decrease of the expression of undifferentiated ES cell marker genes, such as *Nanog*, *Eras*, and *Oct3/4*, and the up-regulation of neural markers such as *Sox1*, *βIII-tubulin*, and *GFAP* during the neural differentiation of 38C2 iPS cells, similar to EB3 ES cells (Fig. 1*D*).

Moreover, electrophysiological analysis using whole-cell patch clamping in both the 38C2 iPS-PNS– and EB ES-PNS–derived neurons after 21–28 d of adherent differentiation showed tetrodotoxin (TTX; 1 μM)-sensitive repetitive action potentials in the current-clamp mode [38C2 iPS-PNS (n = 11 of 16) and EB3 ES-PNS (n = 5 of 7)] (Fig. S2*A*) and very rapid inward currents immediately followed by transient outward currents in voltage-clamp mode (Fig. S2*B* 1 and 2). Steady outward currents, similar to those mediated by delayed-rectifier K$^+$ channels, were also observed (Fig. S2 *B*1 and *D*). These findings suggest that 38C2 iPS-PNSs produced neuronal cells equipped with functional channels that could generate and modify action potentials (*SI Text*).

Safe MEF-iPS Cells Can Differentiate into Trilineage Neural Cells in the Injured Spinal Cord Without Tumorigenesis. Previously, we confirmed that SNSs from the safe 38C2 MEF-iPS cell clone survived and showed no teratoma-forming activity in the NOD/SCID mouse brain for 24 wk after transplantation (27) (Fig. S3). 38C2 iPS-SNSs that were transplanted into the intact spinal cord survived and differentiated into trilineage neural cells without any tumorigenesis (Fig. S4). Next, to evaluate their therapeutic effects in the mouse SCI model, we transplanted 38C2 iPS-SNSs into the contused spinal cord 9 d after injury and compared them with EB3 ES-SNSs, using adult fibroblasts and PBS as controls. We also made a comparison with 38C2 iPS-PNSs, because we recently confirmed that the transplantation of ES cell-derived SNSs, but not PNSs, provides therapeutic benefit after SCI (31). We transplanted 38C2 iPS-SNSs that had been prelabeled by lentivirus to express both CBR*luc* and mRFP (32, 33) into the lesion epicenter 9 d after the injury. Bioluminescence imaging (BLI) analysis (34), which detects luciferase photon signals only from living cells, revealed an approximate graft survival rate of 18% at 35 d after transplantation (Fig. 2*A*). We also histologically confirmed that the grafted cells survived and exhibited no apparent evidence of tumorigenesis (Fig. 2*B*), and that there were no Nanog$^+$ cells (Fig. S5), at least during our observation

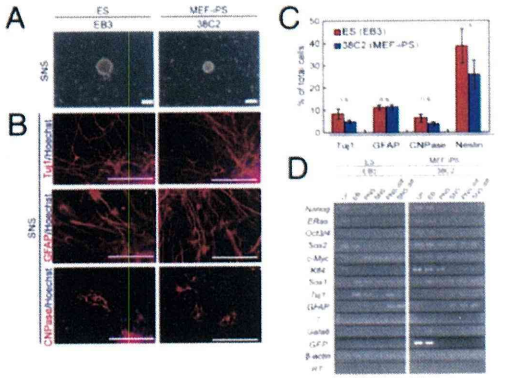

Fig. 1. Neural differentiation of pre-evaluated safe MEF-iPS cells in vitro. (*A*) Neurospheres derived from EB3 ES cells and 38C2 iPS cells. (Scale bar: 200 μm.) (*B*) Immunocytochemical analysis of neural cell marker proteins in the differentiated SNSs derived from EB3 ES and 38C2 iPS cells. (Scale bar: 100 μm.) (*C*) Neural differentiation efficiencies of neurospheres derived from EB3 ES and 38C2 iPS cells. (n = 5, n.s.). (*D*) RT-PCR analysis of undifferentiated cells (Un.), EBs, PNSs, SNSs, differentiated PNSs (PNS diff.), and SNSs (SNS diff.) of the EB3-ES and 38C2 iPS cells.

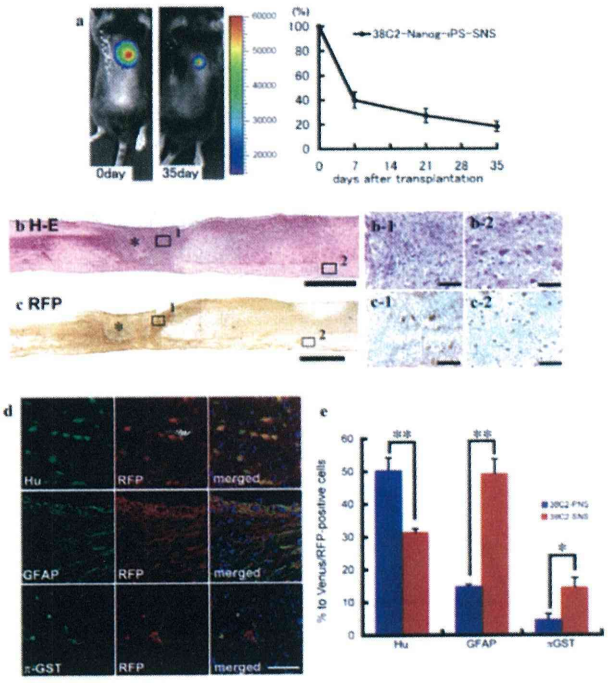

Fig. 2. Transplanted SNSs derived from safe MEF-iPS clones survive without any evidence of tumorigenesis and differentiate into trilineage neural cells in the injured spinal cord. (*A*) Representative BLI images of a mouse in which CBR*luc*-expressing 38C2 iPS-SNSs were transplanted into the injured spinal cord (*Left*, immediately after transplantation; *Right*, 42 d after transplantation). Quantification of the photon intensity revealed that ≈60% of the grafted cells were lost within 7 d after transplantation, and ≈20% of the cells survived 35 d after transplantation. Values are means ± SEM (n = 6). (*B*) H&E and (*C*) anti-RFP DAB staining of sagittal sections of the spinal cord 42 d after injury (38C2 iPS-SNS transplanted). There was no evidence of tumorigenesis (*B*). No significant nuclear atypia was observed in magnified images of the boxed areas showing the lesion epicenter (*B*-1) or white matter caudal to the transplantation site (*B*-2). Grafted cells survived and were diffusely distributed rostral and caudal to the lesion site (*C*). Higher-magnification images of the boxed areas showing the lesion site (*C*-1) and white matter caudal to the lesion site (*C*-2). *Lesion epicenter. (*D*) Immunohistochemical analyses of 38C2 iPS-SNSs grafted into spinal cord 42 d after injury, revealing grafted cells double-positive for RFP and markers of neural lineages. (*E*) Quantitative analyses of Hu$^+$ neurons, GFAP$^+$ astrocytes, and π-GST$^+$ oligodendrocytes. Values are means ± SEM (n = 3 each; *P < 0.05, **P < 0.01).

period. Grafted RFP$^+$ cells were located mainly around the lesion epicenter, whereas some cells had migrated as far as 4 mm rostral and caudal to the graft site (Fig. 2*C*). In the injured spinal cord, the grafted 38C2 iPS-SNSs differentiated into three types of neural cells, including Hu$^+$ neurons (31.4 ± 1.1%), GFAP$^+$ astrocytes (49.3 ± 4.5%), and π-GST$^+$ oligodendrocytes (14.4 ± 3.0%), whereas 38C2 iPS-PNSs differentiated dominantly into neurons—that is, Hu$^+$ neurons (50.4 ± 3.8%), GFAP$^+$ astrocytes (14.9 ± 0.6%), and π-GST$^+$ oligodendrocytes (4.6 ± 1.8%) (Fig. 2 *D* and *E* and Fig. S6).

Transplantation of SNSs Derived from Safe MEF-iPS Cells into the Injured Spinal Cord Promotes Functional Recovery. The contusive SCI initially caused complete paralysis, followed by gradual recovery that reached a plateau. There were statistically significant differences in Basso mouse scale (BMS) between the 38C2 iPS-SNS and PBS groups at 21, 28, 35, and 42 d after injury, whereas no significant difference was observed between the 38C2 iPS-SNS and EB3 ES-SNS groups. Forty-two days after injury, the 38C2 iPS-SNS–grafted animals could lift their trunks and had significantly better BMS than the PBS control or adult fibroblast-treated animals, which were unable to support their body weight with their hindlimbs (Fig. 3*A*). To reveal the potential mechanism of functional recovery after 38C2 iPS-SNS transplantation, we conducted further histological analyses. By Luxol Fast Blue (LFB) staining, 38C2 iPS-SNS–grafted mice showed a significantly larger myelinated area at the lesion epicenter than the PBS control mice at 42 d after injury (Fig. 3*B*). We also found that grafted 38C2 iPS-SNS–derived cells myelinated NF200$^+$ host neuronal fibers, confirmed by the positive staining of RFP and myelin basic protein (MBP; Fig. 3*C*), indicating that graft cell-derived oligodendrocytes were capable of remyelination. For further confirmation of the myelinating ability of 38C2 iPS-SNSs, we transplanted 38C2 iPS-SNSs into the injured spinal cord of MBP-null *shiverer* mice, a severely hypo- and dysmyelinating mutant mouse that lacks the major dense line of CNS myelin (35). Myelinating potential of the grafted 38C2 iPS-SNS–derived cells was confirmed, exhibiting MBP$^+$ deposits (Fig. 3*D*) and the major dense line, by electron microscopic analysis (Fig. 3*E*).

To determine the effect of the grafted 38C2 iPS-SNSs on serotonergic nerve fibers, which are important for the motor functional recovery of hind limbs (36, 37), we immunostained for 5HT and quantified the positive area at the distal cord 1, 2, and 6 wk after injury. Some of the nerve fibers associated with graft cell-derived Hu$^+$ neurons were identified as 5HT$^+$ serotonergic fibers, and were prominent at the distal cord compared with the PBS control group (Fig. 4 *A–C*). Quantitative analysis of the serotonergic innervation of the distal cord revealed a significant difference between the 38C2 iPS-SNS and PBS control groups (Fig. 4*B*). The contusive injury (60 kDyn) resulted in a significant decrease in the number of 5HT$^+$ fibers at the distal cord, followed by a slight recovery, which is the nature of contusive SCI. The injection of PBS in the PBS control group did not induce any additional increase in the number of 5HT$^+$ fibers at the distal cord. In contrast, innervation of the distal cord by these 5HT$^+$ fibers was enhanced by the grafted 38C2 iPS-SNS 6 wk after SCI (Fig. 4*B*). Moreover, 38C2 iPS-SNS–derived astrocytes, which exhibited a bipolar morphology with long processes, were observed closely associated with the 5HT$^+$ serotonergic fibers (Fig. 4*D*).

Transplantation of Neurospheres Derived from Pre-Evaluated Safe or Unsafe TTF-iPS Cells into the Injured Spinal Cord. Toward the goal of clinical application, we next examined the therapeutic potential

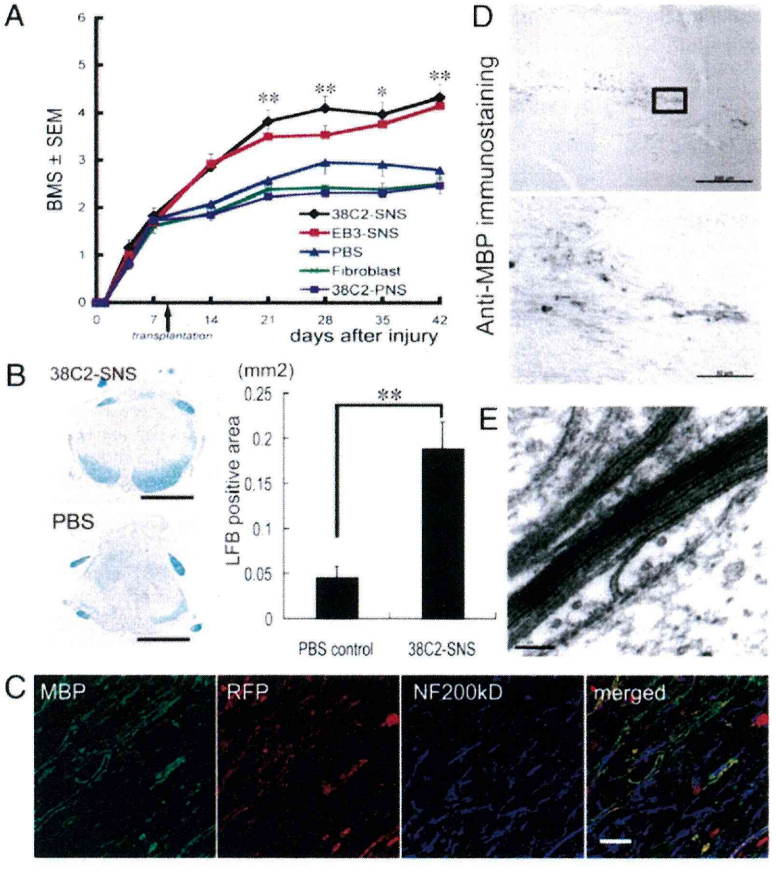

Fig. 3. SNS derived from a safe MEF-iPS clone differentiate into mature oligodendrocytes and promote remyelination. (*A*) Time course of functional recovery of hind limbs evaluated by BMS. 38C2 iPS-SNS, $n = 19$; EB3 ES-SNS, $n = 15$; PBS, $n = 12$; adult fibroblasts, $n = 13$; 38C2 iPS-PNS, $n = 13$. $^*P < 0.05$, $^{**}P < 0.01$. (*B*) LFB staining of axial sections of the spinal cord at the lesion epicenter 42 d after injury; 38C2 iPS-SNS–transplanted (*Upper Left*) and PBS control (*Lower Left*) animals. Quantification of LFB-positive areas at the lesion epicenter 42 d after injury (*Right*, $n = 7$ each; $^{**}P < 0.01$). (*C*) Immunohistochemistry of 38C2 iPS-SNS–derived mature oligodendrocytes (MBP$^+$). Grafted cells were integrated into myelin sheath. (*D*) Anti-MBP DAB staining of sagittally sectioned spinal cord of a *shiverer* mouse 8 wk after transplantation. MBP$^+$ myelin was detected in the area caudal to the lesion epicenter. (*Lower*) Higher-magnification image of the boxed area. (*E*) EM pictures of the injured spinal cord of a 38C2 iPS-SNS–grafted *shiverer* mouse exhibiting a prominent major dense line and intraperiod lines in multiple compacted lamellae. (Scale bars: *B*, 500 μm; *D Upper*, 200 μm; *C* and *D Lower*, 50 μm; and *E*, 0.1 μm.)

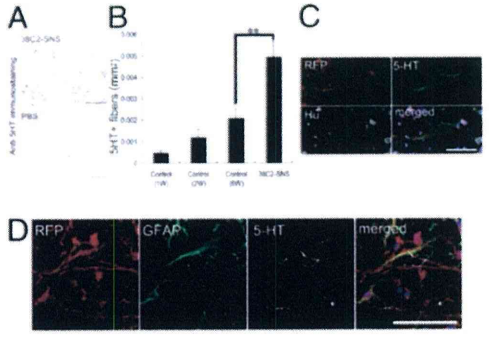

Fig. 4. SNSs derived from a safe MEF-iPS clone promote serotonergic innervation of the dorsal cord and result in better functional recovery of the hindlimbs. (*A*) 38C2 iPS-SNS transplantation promoted the growth of 5HT$^+$ serotonergic fibers in the distal spinal cord. Axial sections of 38C2 iPS-SNS–transplanted (*Upper*) and PBS control mice (*Lower*). (*B*) Quantitative analysis of 5HT$^+$ serotonergic fibers of distal cord in the PBS control (1, 2, and 6 wk postinjury) and 38C2 iPS-SNS transplantation groups (6 wk postinjury; 1 and 2 wk postinjury, $n = 3$ each; 6 wk postinjury and 38C2 SNS, $n = 7$ each; $^{**}P < 0.01$). (*C* and *D*) Immunohistochemistry of 38C2 iPS-SNS–derived neurons (*C*, RFP$^+$, Hu$^+$) and astrocytes (*D*, RFP$^+$, GFAP$^+$) closely associated with 5HT$^+$ serotonergic fibers. (Scale bars: *A*, 100 μm; *C*, 20 μm; *D*, 50 μm.)

of adult tissue-derived iPS cells. Among six TTF-iPS clones pre-evaluated in our previous study (27), we used the safe 335D1 TTF-iPS clone, which was generated with *Nanog* selection and without the transduction of c-Myc. We also used the unsafe 256H13 and 256H18 TTF-iPS clones (22, 27), which were generated without genetic selection or the transduction of c-Myc, and were originally established from CAG-EGFP mice (22). A subclone of RF8 ES cells carrying the *Nanog*-EGFP reporter (1A2) (19) was used as control. All of the TTF-iPS clones formed PNSs and SNSs (Fig. 5*A*), and generated cells of all three neural lineages, similar to those derived from 1A2 ES cells (Fig. 5*B*). We transplanted these TTF-iPS–derived SNSs into injured spinal cords 9 d after injury. Transplantation of the safe 335D1 iPS-SNS (prelabeled with RFP lentivirally) resulted in better functional recovery compared with the PBS control group, without any apparent tumorigenesis during our observation period (Fig. 5 *C* and *D*). Grafted and survived RFP$^+$ 335D1 iPS-SNS–derived cells could differentiate into neural trilineages (Fig. S7 *A* and *B*). Furthermore, LFB staining revealed that 335D1 iPS-SNS–grafted mice had a significantly larger myelinated area at the lesion epicenter than the PBS control mice at 42 d after injury (Fig. S8 *A* and *B*), and grafted RFP$^+$ 335D1 SNS-derived cells differentiated into MBP$^+$ oligodendrocytes (Fig. S8*C*). However, all unsafe 256H18 iPS-SNS–grafted mice and one of 256H13 iPS-SNS–grafted mice formed teratomas containing EGFP$^+$ donor cells within the injured spinal cord (Fig. 5 *E* and *F* and Fig. S7*C*). Histological analyses revealed that these teratomas contained epithelial and smooth muscle tissue (Fig. S9*A*), and also exhibited Nanog immunoreactivity (Fig. 5*G*). Although the motor functions gradually recovered in both groups to the same extent as in the safe 335D1 iPS-SNS recipients until 35 d after injury, the 256H18 iPS-SNS–grafted animals exhibited a sudden deterioration of motor function 42 d after injury. In contrast, the 256H13 iPS-SNS–grafted animals maintained their functional recovery at 42 d after injury (Fig. 5*C*). Notably, in most mice of the 256H13 iPS-SNS group, scattered small clusters of Nanog$^+$ cells were observed in the spinal cords without obvious teratoma formation (Fig. S9 *B* and *C*). Thus, we speculate that teratoma formation and subsequent deterioration of function recovery would occur in the 256H13 group if a longer observation period was set.

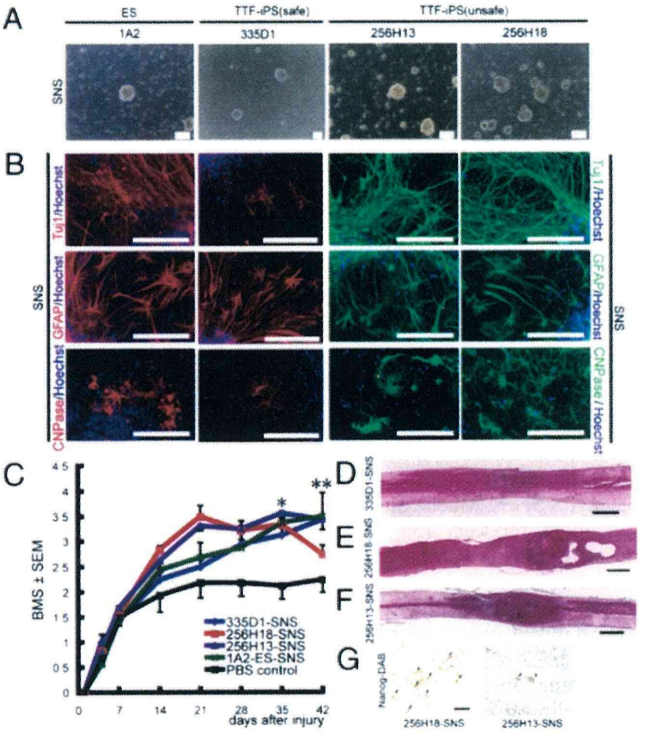

Fig. 5. Characterization and transplantation of SNSs derived from safe and unsafe TTF-iPS cells. (*A*) Neurospheres derived from 1A2 ES cells, 335D1, 256H13, and 256H18 iPS cells. (Scale bar: 200 μm.) (*B*) The differentiation potential of TTF-iPS-derived SNSs tested in vitro by immunocytochemical analyses of neural cell markers; Tuj1 for neurons, GFAP for astrocytes, and CNPase for oligodendrocytes. (Scale bar: 100 μm.) (*C*) Time course of functional recovery of the hindlimbs evaluated by BMS. 335D1 iPS-SNS: $n = 9$ each; 256H13 and 256H18 iPS-SNS: $n = 9$; 1A2 ES-SNS: $n = 9$; PBS control: $n = 8$. $^*P < 0.05$, $^{**}P < 0.01$. (*D–F*) H&E sagittal sections of the spinal cord 42 d after injury. (*D*) 335D1 iPS-SNS, (*E*) 256H18 iPS-SNS, and (*F*) 256H13 iPS-SNS grafted mice. There was no evidence of tumorigenesis in the 335D1 iPS-SNS grafted mice (*D*), whereas teratoma formation was detected within the injured spinal cord in both 256H18 iPS-SNS (*E*), and 256H13 iPS-SNS (*F*) grafted mice. (*G*) Anti-Nanog DAB staining of sagittally sectioned spinal cord of 256H18 and 256H13 iPS-SNS–transplanted animals 35 d after transplantation.

Discussion

In the present study, we showed that the pre-evaluated safe iPS cells could produce neurospheres containing NS/PCs (Fig. 1*A*) that give rise to trilineage neural cells, including several types of neurons (Fig. 1 *B* and *C*), and that the neurons were electrophysiologically functional in vitro similar to ES cells (Fig. S2).

Based on these safety assessments and in vitro findings, we performed an in vivo study using the safe 38C2 MEF-iPS cell clone. Grafted 38C2 iPS-SNSs differentiated into neurons, astrocytes, and oligodendrocytes without forming teratomas or other tumors, and promoted functional recovery after SCI, whereas 38C2 iPS-PNSs did not show any therapeutic effects (Fig. 3*A*). These findings were compatible with our recent data on mouse ES cell-derived neurosphere transplantation into an identical mouse SCI model (31). Transplantation of ES-derived SNSs, which can differentiate into neural trilineages, promoted remyelination, axonal regrowth and tissue sparing, leading to improved function. In contrast, predominantly neurogenic PNSs showed no therapeutic effects on SCI (31). Thus, we elected to use iPS-SNSs and not iPS-PNSs for this study. In fact, the grafted 38C2 iPS-SNSs formed MBP$^+$ myelin sheaths within the injured spinal cord. We also confirmed the myelination potential of 38C2 iPS-SNS–derived cells in the spinal cord of the MBP-null *shiverer* mouse by electron microscopy (Fig. 3

D and *E*). These findings suggested the possibility of the remyelination of demyelinated axons by the grafted 38C2 iPS-SNS–derived oligodendrocytes, which may have contributed to the functional recovery of the grafted animals.

Another potential mechanism for functional recovery is axonal regrowth supported by iPS-SNS–derived astrocytes. Here, we observed grafted 38C2 iPS-SNS–derived $GFAP^+$ astrocytes, which exhibited a bipolar morphology with long processes extending along the axis of the spinal cord, caudal to the lesion epicenter, in close association with $5HT^+$ host serotonergic fibers (Fig. 4*D*). A previous report indicated that immature astrocytes derived from cells grafted into the injured spinal cord promote the outgrowth of $5HT^+$ fibers by offering a growth-permissive surface (38). Consistent with this finding, the transplantation of 38C2 iPS-SNSs promoted serotonergic innervation of the distal cord compared with the PBS control animals, thereby enhancing functional recovery after SCI (Fig. 4 *A* and *B*) (36). Furthermore, trophic factors, such as neurotrophin-3 (NT-3) and brain-derived neurotrophic factor (BDNF), were expressed in 38C2 iPS-SNSs, which could act as an integral part of the observed functional recovery (39, 40). The tissue sparing (e.g., neuroprotection, axon sprouting and remyelination) and other effects, including functional remodeling of spinal locomotor circuits (41), of trophic factors secreted from grafted cells are considered to be important for functional recovery (42). Thus, the combined effects of the 38C2 iPS-SNS–derived glial cells probably contributed to locomotor function recovery.

For clinical applications, the findings with TTF-iPS cells were promising, as most SCI patients are adults. The transplantation of SNSs derived from a pre-evaluated safe TTF-iPS clone promoted functional recovery after SCI without teratoma formation, like the SNSs from safe MEF-iPS clone did (Fig. 5*D*). However, the transplantation of SNSs derived from the unsafe TTF-iPS cells resulted in teratoma formation and functional deterioration. The teratoma-forming activity of TTF-iPS-SNSs could be caused by the presence of undifferentiated cells that might be resistant to differentiation signals within the SNSs (27). In fact, we recently reported that persistent presence of undifferentiated cells within iPS-SNSs highly correlated with teratoma-forming propensity, assayed by flow cytometric analysis using *Nanog*-EGFP reporter and transplantation into the brains of immunodeficient (NOD/SCID) (27). Before iPS cells of adult origin can be used clinically, important hurdles must still be overcome. Though new methods for establishing iPS cells are constantly being developed, including virus-free (43) and transgene-free (44) systems, a new strategy is needed to exclude undifferentiated cells from the differentiated progeny of iPS cells. These findings show that the pre-evaluation of iPS cells' in vitro differentiation potential could play a critical role in terms of their safety and therapeutic effects on the mouse SCI model. Thus, iPS-derived neurosphere transplantation has potential therapeutic use in SCI, when the iPS cell clones are carefully pre-evaluated.

From a clinical viewpoint, it is particularly encouraging that delaying the iPS-derived NS/PC transplantation (to 9 d after injury) enhanced both the survival of the grafted cells and functional recovery, the therapeutic effects of which is almost comparable to those of fetal CNS-derived NS/PCs transplantation (refs. 34 and 45). This finding may also be applicable to the treatment of patients with SCI. Since our first report of iPS cells (18), there has been increasing interest in their characteristics and therapeutic potential. Our present study demonstrates the therapeutic potential of iPS-derived NS/PCs for SCI repair. Before any clinical trial of human CNS disorders using iPS cells, it will be essential to pre-evaluate each iPS cell clone carefully to guarantee a safety level equal to other types of cells, such as Schwann cells (46, 47) and fetal-derived neurosphere cells (NS/PCs) (3), and to conduct preclinical transplantation studies using appropriate primate models (48, 49).

Methods

Reverse-Transcription and RT-PCR. RNA was isolated with TRIzol (Invitrogen) according to the manufacturer's instructions. Total RNA (0.5 μg) was treated with TURBO DNase (Ambion) and then reverse-transcribed with oligo (dT) primer and SuperScript III (Invitrogen). The primers and PCR conditions used in this study are listed Table S1.

Cell Culture, Neural Induction, and Immunocytochemistry. Mouse ES and iPS cells were cultured as described previously (19, 28, 29). Mouse ES and iPS cells were differentiated into neurospheres via EBs treated with 10^{-8} M retinoic acid (Sigma), as described previously with minor modification (28, 29). (Detailed differentiation protocol is described in *SI Text*.) ES and iPS cell-derived neurospheres were dissociated and differentiated on poly-L-ornithine/fibronectin-coated coverslips for 5 d and subjected to immunocytochemical analysis. The number of cells immunoreactive for each marker was counted and shown as the percentage of the total number of cells counterstained with Hoechst 33258. The antibodies used in this study are listed in Table S2.

Lentivirus Production and Infection of Secondary Neurospheres. For BLI tracing of grafted 38C2 iPS-SNSs, we generated a modified lentivirus vector encoding both the click beetle red luciferase (CBR*luc*; Promega) and mRFP, pCSII-EF-CBR*luc*-IRES2-mRFP (32, 33). For lentivirus preparation, HEK-293T cells were transfected with pCSII-EF-CBR*luc*-IRES2-mRFP, pCAG-HIVgp, and pCMV-VSV-G-RSV-Rev, and the conditioned medium containing virus particles was concentrated and used for viral transduction.

Spinal Cord Injury Model and Transplantation. Adult female C57BL/6J mice (20–22 g) were anesthetized via an i.p. injection of ketamine (100 mg/kg) and xylazine (10 mg/kg). A contusive spinal cord injury using an Infinite Horizon Impactor (60 kdyn; Precision Systems) was induced at the Th10 level as reported previously (34). For transplantation, 5×10^5 cells of mouse ES/iPS cell-derived neurospheres, adult dermal fibroblasts in 2 μL of cell suspension, or PBS was injected into the lesion epicenter. Hindlimb motor function was evaluated by the locomotor rating of the Basso mouse scale (BMS) (50) for 42 d after injury. For the in vivo imaging of intact and injured spinal cords after the transplantation, a Xenogen-IVIS 100 cooled CCD optical macroscopic imaging system (SC BioScience) was used for BLI, as reported previously (34) (*SI Text*). All procedures were approved by the ethics committee of Keio University, and were in accordance with the Guide for the Care and Use of Laboratory Animals (National Institutes of Health). Grafted animals were deeply anesthetized and intracardially perfused with 4% paraformaldehyde (PFA; pH 7.4). The dissected spinal cords were sectioned into 20-μm axial/sagittal sections using a cryostat and processed for histological analyses. Detailed conditions for histological analyses are described in *SI Text*.

Statistical Analysis. All data are reported as the mean ± SEM. An unpaired two-tailed Student's *t* test was used for the analyses of in vitro and in vivo 38C2 iPS-SNS and ES-SNS differentiation efficiency (Figs. 1*C* and 2*E*), $5HT^+$ areas (Fig. 4*B*), and LFB^+ areas (Fig. 2*B*). Repeated-measures two-way ANOVA, followed by the Tukey–Kramer test, was used for BMS analysis. $*P < 0.05$, $**P < 0.01$.

ACKNOWLEDGMENTS. We thank Drs. H. Abe, T. Sunabori, F. Renault-Mihara, W. Akamatsu, S. Shibata, T. Harada, S. Miyao, and H. J. Okano (Keio University) for technical assistance and scientific discussions, and all the members of Dr. Okano's and Dr. Yamanaka's laboratories for encouragement and generous support. We also thank Drs. K. Okita, M. Koyanagi, and K. Tanabe (Kyoto University) for the undifferentiated iPS cells, Dr. H. Niwa (Riken CDB) for the EB3 ES cells, Dr. R. Farese (University of California-San Francisco) for the RF8 ES cells, Dr. R. Y. Tsien (University of California-San Diego) for the mRFP gene, Dr. A. Miyawaki (Riken BSI) for the Venus gene, Dr. H. Baba (Tokyo University of Phamacy and Life Science) for the shiverer mice, and Dr. H. Miyoshi (Riken BRC) for the lentiviral vectors. We especially thank Drs. S. Okada (Kyusyu University), A. Iwanami (University of California-San Francisco and Keio University), and J. Yamane (Keio University) for scientific discussions, technical advice, and encouragement. This work was supported by grants from the Program for Promotion of Fundamental Studies in Health Sciences of the National Institute of Biomedical Innovation (NIBIO), a grant from Uehara Memorial Foundation, and Grants-in-Aid for Scientific Research from the Japan Society for the Promotion of Science (JSPS) and the Ministry of Education, Culture, Sports, Science and Technology of Japan (MEXT), the project for realization of regenerative medicine and support for the core institutes for iPS cell research from MEXT; Japan Science and Technology Agency (SORST); the Ministry of Health, Labor, and Welfare; the General Insurance Association of Japan; Research Fellowships for Young Scientists from the Japan Society for the Promotion of Science; Keio Gijuku Academic Development Funds; and a Grant-in-aid for the Global COE program from MEXT to Keio University.

1. Björklund A, Lindvall O (2000) Cell replacement therapies for central nervous system disorders. *Nat Neurosci* 3:537–544.
2. Okano H (2002) Stem cell biology of the central nervous system. *J Neurosci Res* 69: 698–707.
3. Lindvall O, Kokaia Z, Martinez-Serrano A (2004) Stem cell therapy for human neurodegenerative disorders—how to make it work. *Nat Med* 10 (Suppl):S42–S50.
4. Martino G, Pluchino S (2006) The therapeutic potential of neural stem cells. *Nat Rev Neurosci* 7:395–406.
5. Lindvall O, Kokaia Z (2006) Stem cells for the treatment of neurological disorders. *Nature* 441:1094–1096.
6. Gage FH (2000) Mammalian neural stem cells. *Science* 287:1433–1438.
7. Wichterle H, Lieberam I, Porter JA, Jessell TM (2002) Directed differentiation of embryonic stem cells into motor neurons. *Cell* 110:385–397.
8. Watanabe K, et al. (2005) Directed differentiation of telencephalic precursors from embryonic stem cells. *Nat Neurosci* 8:288–296.
9. Sonntag KC, et al. (2007) Enhanced yield of neuroepithelial precursors and midbrain-like dopaminergic neurons from human embryonic stem cells using the bone morphogenic protein antagonist noggin. *Stem Cells* 25:411–418.
10. Tropepe V, et al. (2001) Direct neural fate specification from embryonic stem cells: A primitive mammalian neural stem cell stage acquired through a default mechanism. *Neuron* 30:65–78.
11. Ying QL, Stavridis M, Griffiths D, Li M, Smith A (2003) Conversion of embryonic stem cells into neuroectodermal precursors in adherent monoculture. *Nat Biotechnol* 21: 183–186.
12. McDonald JW, et al. (1999) Transplanted embryonic stem cells survive, differentiate and promote recovery in injured rat spinal cord. *Nat Med* 5:1410–1412.
13. Brüstle O, et al. (1999) Embryonic stem cell-derived glial precursors: A source of myelinating transplants. *Science* 285:754–756.
14. Kim JH, et al. (2002) Dopamine neurons derived from embryonic stem cells function in an animal model of Parkinson's disease. *Nature* 418:50–56.
15. Sharp J, Keirstead HS (2007) Therapeutic applications of oligodendrocyte precursors derived from human embryonic stem cells. *Curr Opin Biotechnol* 18:434–440.
16. Keirstead HS, et al. (2005) Human embryonic stem cell-derived oligodendrocyte progenitor cell transplants remyelinate and restore locomotion after spinal cord injury. *J Neurosci* 25:4694–4705.
17. Hochedlinger K, Jaenisch R (2006) Nuclear reprogramming and pluripotency. *Nature* 441:1061–1067.
18. Takahashi K, Yamanaka S (2006) Induction of pluripotent stem cells from mouse embryonic and adult fibroblast cultures by defined factors. *Cell* 126:663–676.
19. Okita K, Ichisaka T, Yamanaka S (2007) Generation of germline-competent induced pluripotent stem cells. *Nature* 448:313–317.
20. Wernig M, et al. (2007) In vitro reprogramming of fibroblasts into a pluripotent ES-cell-like state. *Nature* 448:318–324.
21. Maherali N, et al. (2007) Directly reprogrammed fibroblasts show global epigenetic remodeling and widespread tissue contribution. *Cell Stem Cell* 1:55–70.
22. Nakagawa M, et al. (2008) Generation of induced pluripotent stem cells without Myc from mouse and human fibroblasts. *Nat Biotechnol* 26:101–106.
23. Wernig M, Meissner A, Cassady JP, Jaenisch R (2008) c-Myc is dispensable for direct reprogramming of mouse fibroblasts. *Cell Stem Cell* 2:10–12.
24. Hanna J, et al. (2007) Treatment of sickle cell anemia mouse model with iPS cells generated from autologous skin. *Science* 318:1920–1923.
25. Wernig M, et al. (2008) Neurons derived from reprogrammed fibroblasts functionally integrate into the fetal brain and improve symptoms of rats with Parkinson's disease. *Proc Natl Acad Sci USA* 105:5856–5861.
26. Yamanaka S (2007) Strategies and new developments in the generation of patient-specific pluripotent stem cells. *Cell Stem Cell* 1:39–49.
27. Miura K, et al. (2009) Variation in the safety of induced pluripotent stem cell lines. *Nat Biotechnol* 27:743–745.
28. Okada Y, et al. (2008) Spatiotemporal recapitulation of central nervous system development by murine embryonic stem cell-derived neural stem/progenitor cells. *Stem Cells* 26:3086–3098.
29. Okada Y, Shimazaki T, Sobue G, Okano H (2004) Retinoic-acid-concentration-dependent acquisition of neural cell identity during in vitro differentiation of mouse embryonic stem cells. *Dev Biol* 275:124–142.
30. Niwa H, Miyazaki J, Smith AG (2000) Quantitative expression of Oct-3/4 defines differentiation, dedifferentiation or self-renewal of ES cells. *Nat Genet* 24:372–376.
31. Kumagai G, et al. (2009) Roles of ES cell-derived gliogenic neural stem/progenitor cells in functional recovery after spinal cord injury. *PLoS ONE* 4:e7706.
32. Masuda H, et al. (2007) Noninvasive and real-time assessment of reconstructed functional human endometrium in NOD/SCID/gamma c(null) immunodeficient mice. *Proc Natl Acad Sci USA* 104:1925–1930.
33. Miyoshi H, Blömer U, Takahashi M, Gage FH, Verma IM (1998) Development of a self-inactivating lentivirus vector. *J Virol* 72:8150–8157.
34. Okada S, et al. (2005) In vivo imaging of engrafted neural stem cells: Its application in evaluating the optimal timing of transplantation for spinal cord injury. *FASEB J* 19: 1839–1841.
35. Inoue Y, et al. (1986) Alteration of the primary pattern of central myelin in a chimaeric environment—study of shiverer ↔ wild-type chimaeras. *Brain Res* 391:239–247.
36. Bregman BS, et al. (1993) Recovery of function after spinal cord injury: Mechanisms underlying transplant-mediated recovery of function differ after spinal cord injury in newborn and adult rats. *Exp Neurol* 123:3–16.
37. Nygren LG, Fuxe K, Jonsson G, Olson L (1974) Functional regeneration of 5-hydroxytryptamine nerve terminals in the rat spinal cord following 5, 6-dihydroxytryptamine induced degeneration. *Brain Res* 78:377–394.
38. Hofstetter CP, et al. (2002) Marrow stromal cells form guiding strands in the injured spinal cord and promote recovery. *Proc Natl Acad Sci USA* 99:2199–2204.
39. Widenfalk J, Lundströmer K, Jubran M, Brene S, Olson L (2001) Neurotrophic factors and receptors in the immature and adult spinal cord after mechanical injury or kainic acid. *J Neurosci* 21:3457–3475.
40. McTigue DM, Horner PJ, Stokes BT, Gage FH (1998) Neurotrophin-3 and brain-derived neurotrophic factor induce oligodendrocyte proliferation and myelination of regenerating axons in the contused adult rat spinal cord. *J Neurosci* 18:5354–5365.
41. Courtine G, et al. (2009) Transformation of nonfunctional spinal circuits into functional states after the loss of brain input. *Nat Neurosci* 12:1333–1342.
42. Lu P, Tuszynski MH (2008) Growth factors and combinatorial therapies for CNS regeneration. *Exp Neurol* 209:313–320.
43. Okita K, Nakagawa M, Hyenjong H, Ichisaka T, Yamanaka S (2008) Generation of mouse induced pluripotent stem cells without viral vectors. *Science* 322:949–953.
44. Zhou H, et al. (2009) Generation of induced pluripotent stem cells using recombinant proteins. *Cell Stem Cell* 4:381–384.
45. Ogawa Y, et al. (2002) Transplantation of in vitro-expanded fetal neural progenitor cells results in neurogenesis and functional recovery after spinal cord contusion injury in adult rats. *J Neurosci Res* 69:925–933.
46. Pearse DD, et al. (2004) cAMP and Schwann cells promote axonal growth and functional recovery after spinal cord injury. *Nat Med* 10:610–616.
47. Pearse DD, et al. (2007) Transplantation of Schwann cells and/or olfactory ensheathing glia into the contused spinal cord: Survival, migration, axon association, and functional recovery. *Glia* 55:976–1000.
48. Iwanami A, et al. (2005) Establishment of graded spinal cord injury model in a nonhuman primate: The common marmoset. *J Neurosci Res* 80:172–181.
49. Iwanami A, et al. (2005) Transplantation of human neural stem cells for spinal cord injury in primates. *J Neurosci Res* 80:182–190.
50. Basso DM, et al. (2006) Basso Mouse Scale for locomotion detects differences in recovery after spinal cord injury in five common mouse strains. *J Neurotrauma* 23:635–659.

Journal of Neuroscience Research

Journal of Neuroscience Research 88:2197–2206 (2010)

Antiapoptotic and Antiautophagic Effects of Glial Cell Line-Derived Neurotrophic Factor and Hepatocyte Growth Factor After Transient Middle Cerebral Artery Occlusion in Rats

Jingwei Shang,[1] Kentaro Deguchi,[1] Toru Yamashita,[1] Yasuyuki Ohta,[1] Hanzhe Zhang,[1] Nobutoshi Morimoto,[1] Ning Liu,[1] Xuemei Zhang,[1] Fengfeng Tian,[1] Tohru Matsuura,[1] Hiroshi Funakoshi,[2] Toshikazu Nakamura,[3] and Koji Abe[1]*

[1]Department of Neurology, Okayama University Graduate School of Medicine, Dentistry and Pharmaceutical Sciences, Okayama, Japan
[2]Division of Molecular Regenerative Medicine, Department of Biochemistry and Molecular Biology, Osaka University Graduate School of Medicine, Osaka, Japan
[3]Kringle Pharma Joint Research Division for Regenerative Drug Discovery, Center for Advanced Medicine, Osaka University, Osaka, Japan

Glial cell line-derived neurotrophic factor (GDNF) and hepatocyte growth factor (HGF) are strong neurotrophic factors, which function as antiapoptotic factors. However, the neuroprotective effect of GDNF and HGF in ameliorating ischemic brain injury via an antiautophagic effect has not been examined. Therefore, we investigated GDNF and HGF for changes of infarct size and antiapoptotic and antiautophagic effects after transient middle cerebral artery occlusion (tMCAO) in rats. For the estimation of ischemic brain injury, the infarct size was calculated at 24 hr after tMCAO by HE staining. Terminal deoxynucleotidyl transferase-mediated dUTP-biotin in situ nick end labeling (TUNEL) was performed for evaluating the antiapoptotic effect. Western blot analysis of microtubule-associated protein 1 light chain 3 (LC3) and immunofluorescence analysis of LC3 and phosphorylated mTOR/Ser^{2448} (p-mTOR) were performed for evaluating the antiautophagic effect. GDNF and HGF significantly reduced infarct size after cerebral ischemia. The amounts of LC3-I plus LC3-II (relative to β-tubulin) were significantly increased after tMCAO, and GDNF and HGF significantly decreased them. GDNF and HGF significantly increased p-mTOR-positive cells. GDNF and HGF significantly decreased the numbers of TUNEL-, LC3-, and LC3/TUNEL double-positive cells. LC3/TUNEL double-positive cells accounted for about 34.3% of LC3 plus TUNEL-positive cells. This study suggests that the protective effects of GDNF and HGF were greatly associated with not only the antiapoptotic but also the antiautophagic effects; maybe two types of cell death can occur in the same cell at the same time, and GDNF and HGF are capable of ameliorating these two pathways.

Key words: apoptosis; autophagy; GDNF; HGF; cerebral ischemia

In ischemic diseases, ischemic severity and duration lead to cell death and determine tissue pathology (Cotran et al., 1998). In recent years, new types of cell death have been described; three types of cell deaths have been distinguished mainly by morphological criteria. Type I cell death is better known as apoptosis, and autophagic vacuoles inside the dying cell are typical for type II cell death, whereas type III cell death (better known as necrosis) is distinguished by early plasma membrane rupture and dilation of cytoplasmic organelles (Kroemer, 2005; Galluzzi, 2007; Feig and Peter, 2007). Apoptosis is associated with nuclear and chromatin condensation, DNA fragmentation, organelle swelling, cytoplasmic vacuolization, and nuclear envelope disruption (Kerr et al., 1972; Green and Kroemer, 1998). Autophagy is a regulated process of degradation and recycling of cellular

Contract grant sponsor: Ministry of Education, Science, Culture and Sports of Japan; Contract grant number: 21390267; Contract grant sponsor: Reasearch Committee of CNS Degenerative Diseases (to I. Nakano); Contract grant sponsor: Ministry of Health, Labour and Welfare of Japan (to Y. Itoyama, T. Imai).

*Correspondence to: Koji Abe, Okayama University Graduate School of Medicine, Dentistry and, Pharmaceutical Sciences, 2-5-1 Shikatacho, Okayama 700-8558, Japan. E-mail: abekabek@cc.okayama-u.ac.jp

Received 7 November 2009; Revised 5 December 2009; Accepted 26 December 2009

Published online 19 February 2010 in Wiley InterScience (www.interscience.wiley.com). DOI: 10.1002/jnr.22373

constituents, participating in organelle turnover and in the bioenergetic management of starvation (Kabeya et al., 2000; Klionsky and Emr, 2000; Inbal et al., 2002; Reggiori and Klionsky, 2002; Klionsky et al., 2003; Yoshimori, 2004). Recently, 27 autophagy-related (ATG) genes were identified whose products appear to be related to the autophagy process. These genes were characterized in yeast (Klionsky et al., 2003; Yorimitsu and Klionsky, 2005). For example, rat microtubule-associated protein 1 light chain 3 (LC3), a mammalian homologue of Atg8, plays a critical role in the formation of autophagosomes (Kirisako et al., 1999).

Glial cell line-derived neurotrophic factor (GDNF), a member of the transforming growth factor-β superfamily (Lin et al., 1993), has a potent neuroprotective effect on a variety of neuronal damage both in vitro and in vivo (Lin et al., 1993, 1995; Beck et al., 1995; Tomac et al., 1995; Henderson et al., 1997). We and others have reported that topical application and intracerebral administration of GDNF decreased the size of ischemia-induced brain infarction and the number of TUNEL-positive neurons with suppressing apoptotic pathways such as caspases-1 and -3 (Abe et al., 1997; Wang et al., 1997; Kitagawa et al., 1998).

Hepatocyte growth factor (HGF) is a multifunctional growth factor originally identified as a potent mitogen for hepatocytes in primary culture (Nakamura et al., 1984; Russell et al., 1984). HGF specifically binds and activates a tyrosine kinase receptor encoded by the c-Met protooncogene (Bottaro et al., 1991). Both HGF and c-Met were reported to be expressed in both adult and fetal central nervous system (Matsumoto and Nakamura, 1997; Maina and Klein, 1999). HGF plays important roles in mitogenesis, motogenesis, morphogenesis, antiapoptosis, and angiogenesis (Nakamura et al., 1989; Zarnegar and Michalopoulos, 1995; Matsumoto and Nakamura, 1996; Maina et al., 1998; Van Belle et al., 1998). In the brain, HGF has the functions of a neurotrophic factor via promotion of antiapoptosis, neurite extention, and migration; a modulatory factor for glial cell numbers and function; and an angiogenic factor (Honda et al., 1995; Van Belle et al., 1998; Miyazawa et al., 1998; Sun et al., 2002). We and others have reported that intraventricular and intracerebral administration of HGF protein or transplantation of bone marrow stromal cells with ex vivo HGF gene transfer decreased the size of ischemia-induced brain infarction (Miyazawa et al., 1998; Zhao et al., 2006) and the number of TUNEL-positive neurons with increasing presentation of Bcl-2 (Tsuzuki et al., 2001). In addition, HGF also plays a role in attenuating ischemia-induced brain infarction via caspase-indepent cascade by preventing apoptosis-inducing factor (AIF) translocation downstream of poly(ADP-ribose) polymerase (PARP) and p53 (Niimura et al., 2006a,b).

However, the antiautophagic effect of GDNF and HGF in ameliorating ischemic brain injury has not yet been documented. In this study, we examined the antiapoptotic and antiautophagic effects of GDNF and HGF after tMCAO in rats.

MATERIALS AND METHODS

Surgical Preparation

Adult male Wistar rats (SLC, Shizuoka, Japan) weighing 250–280 g were used for the experiments. The animals were anesthetized with an intraperitoneal injection of 40 mg/kg pentobarbital and positioned in a stereotaxic operating apparatus. A 2-mm-diameter burr hole was carefully made at 3 mm dorsal and 4 mm lateral to the right from bregma using an electric dental drill, avoiding traumatic brain injury. Dura mater was preserved at that time. The location of the burr hole was in the upper part of the right middle cerebral artery (MCA) territory. Then, the incision was closed, and the animals were allowed to free access to water and food at room temperature.

On the next day, at about 24 hr after the drilling, the rats were lightly anesthetized by inhalation of a 69%/30% (v/v) mixture of nitrous oxide/oxygen and 1% halothane using a face mask. A midline neck incision was made and the right common carotid artery exposed, and then inhalation of anesthetics was stopped. When the animal began to regain consciousness, the right MCA was occluded by insertion of 4-0 surgical nylon thread with silicone coating through the common carotid artery (Nagasawa and Kogure, 1989; Abe et al., 1992). With this technique, the tip of the thread occludes the origin of the right MCA. The reliability of producing successful strokes is almost complete in this model (Koizumi et al., 1986). During these procedures, body temperature was monitored with a rectal probe and maintained at 37° ± 0.3°C using a heating pad. The surgical incision was then closed, and the animals were allowed to recover at room temperature. After 90 min of MCA occlusion (MCAO), cerebral blood flow (CBF) was restored by removal of the nylon thread.

HGF or GDNF Treatment In Vivo

Just after restoration of CBF, the dura mater under the burr hole was carefully removed, and a small piece (8 mm^3) of spongel (Yamanouchi Pharma Co., Ltd.) presoaked in 9 μl Ringer solution (Otsuka Pharma. Co., Ltd.) as vehicle or a solution containing GDNF (3.0 μg in 9 μl of vehicle; Sigma, St. Louis, MO) or HGF (30.0 μg in 9 μl of vehicle; Kringle Pharma) was placed in contact with the surface of the cerebral cortex. In terms of the dose of HGF, 5.0, 10.0, and 30.0 μg were checked in our preliminary experiment (Miyazawa et al., 1998; Niimura et al., 2006a,b), and the effect of 30.0 μg in 9 μl of vehicle was the best among them. The dose of GDNF was chosen based on our previous report (Abe et al., 1997). The spongel was buried in the skull bone. The surface of the skull bone was then covered with vinyl tape, and the head skin incision was closed. It is reported that application of growth factor in spongel is as effective as chronic infusion (Otto et al., 1989). The above-described operations were performed in a sterile fashion. Sham-operated control animals underwent burr hole surgery, exposure of the common carotid artery without MCAO, and placement of spongel presoaked in vehicle. The experimental protocol and procedures were approved by the Animal Committee of Okayama University School of Medicine.

Preparation and Quantitative Analysis of Infarct Volume

The animals (n = 5) were sacrificed at 24 hr after the restoration of CBF under deep anesthesia with pentobarbital (10 mg/250 g rat). The rats were transcardially perfused with heparinized saline, followed by 4% paraformaldehyde in phosphate buffer (PB). The whole brain was subsequently removed and immersed in the same fixation for 12 hr at 4°C. After washing out of paraformaldehyde by PB, the brain was immersed in sucrose solution in PB and then rapidly frozen in powdered dry ice and stored at −80°C. Coronal brain sections of 20 μm thickness were prepared by using a cryostat and mounted on a silane-coated glass.

For quantitative analysis of infarct volume, the sections were stained with hematoxylin and eosin (HE) and observed with a light microscope (Olympus BX-51; Olympus Optical). The area of the infarct was measured in fiver sections by pixel counting using a computer program for Photoshop 7.0, and the volume was calculated.

Western Blot Analysis

Western blot analysis was performed using the infarct hemisphere of five mice from each group. We added 3 ml cold lysis buffer (50 mM Tris-HCl, pH 7.2, 10% glycerol, 250 mM NaCl, 0.1% NP-40, 2 mM EDTA, and protease inhibitors) to the brain tissue and homogenized it at 4°C. The homogenate was centrifuged at 12,000 rpm at 4°C, and the supernatant was used for Western blotting. We carried out Western blot analysis using standard techniques with an ECL Plus detection kit (GE Healthcare). The dilution of the anti-LC3 (Medical Biological Laboratories; No. PD012) antibody was 1:500. We carried out densitometry analysis in Scion Image Beta 4.02 software and took the average of the five mice.

TUNEL Staining

In accordance with our previous report (Abe et al., 1997), TUNEL study was performed using a kit (Roche, Nonnenwald, Germany) that detects double-strand breaks in genomic DNA with diaminobenzidine.

Single Immunofluorescence Analysis

The fresh-frozen sections were fixed for 10 min in ice-cold acetone and air dried. Then, the sections were rinsed three times in PBS (pH 7.4). After blocking with 10% normal rabbit serum for 2 hr, the slides were incubated for 16 hr at 4°C with the first antibody: anti-LC3 antibody (MBL; No. PM046) at 1:200 or anti-p-mTOR antibody (Cell Signaling Technologies, Danvers, MA; No. 2971) at 1:100 diluted in PBS containing 10% normal rabbit serum and 0.3% Triton X-100. To confirm the specificity of the primary antibody, a set of sections was stained in a similar way, without primary antibodies. The sections were then washed and incubated for 2 hr with the second antibody: Texas red-labeled anti-rabbit IgG antibody at 1:200 (Vector, Burlingame, CA) or FITC-labeled anti-rabbit IgG antibody at 1:200 (Vector). The slides were then covered with Vectashield Mounting Medium with 4′,6′-diamidino-2-phenylindole (Vector).

Double-Immunofluorescence Analysis

Double-immunofluorescence studies were performed for LC3 plus neuronal nuclear antigen (NeuN) or glial fibrillary acidic protein (GFAP) or TUNEL or N-acetylglucosamine oligomers (NAGO). Lycopersicon esculentum lectin (LEL) is a glycoprotein with affinity for NAGO, which mature vascular endothelial cells express (Augustin et al., 1995). The staining steps were the same as those described above; LEL and the first antibody were chosen with each dilution as follows: anti-LC3 antibody at 1:200, anti-NeuN antibody (Chemicon, Temecula, CA) at 1:200, anti-GFAP antibody (Dako, Carpinteria, CA) at 1:1,000, biotinylated LEL (Vector) at 1:200 diluted in PBS containing 10% normal rabbit serum and 0.3% Triton X-100. The second antibody were Texas red-labeled anti-rabbit IgG antibody at 1:200 (Vector) plus TUNEL enzyme and label or FITC avidin D (Vector) or FITC-labeled secondary antibodies (Vector). The treated sections were scanned with a confocal microscope equipped with an argon and HeNe1 laser (LSM-510; Zeiss, Jena, Germany). Sets of fluorescent images were acquired sequentially for the red and green channels to prevent crossover of signals from green to red or from red to green channels.

Quantitative Analysis

To evaluate the results of TUNEL staining and single-immunofluorescence analysis quantitatively, the positively stained cells were counted in the cerebral cortex at the boundary zone in five coronal sections per rat brain. In the double-fluorescence studies, the double-positive cells and vessels were counted in the same manner. Results are expressed as means ± SD.

Statistical Analysis

All data are expressed as means ± SD. One-way ANOVA with post hoc test was used for each evaluation.

RESULTS

Quantitative Analysis of Infarct Volume

Ninety minutes of MCAO caused large infarcts of the lateral cortex and the underlying caudoputamen. Infarct areas of five coronal sections (2, 4, 6, 8, and 10 mm caudal from frontal pole) are shown (Fig. 1a). The infarct volume of the vehicle-treated group was 478.0 ± 34.8 mm^3 (mean ± SD), HGF-treated group was 420.0 ± 23.8 mm^3, and GDNF-treated group was 306.0 ± 52.2 mm^3. The infarct volume of GDNF (**$P < 0.01$)- and HGF (*$P < 0.05$)-treated groups was significantly smaller than that of vehicle-treated group (Fig. 1b).

Antiapoptotic Effect

The TUNEL-positive stained cells were distributed in the cerebral cortex and dorsal caudate of the MCA territory but were not found in other areas of the ipsilateral hemisphere or the contralateral side. The staining was found exclusively in the nuclei of neuronal cells. A strong staining for TUNEL was present in the vehicle-treated group, but the treatment with GDNF (**$P <$

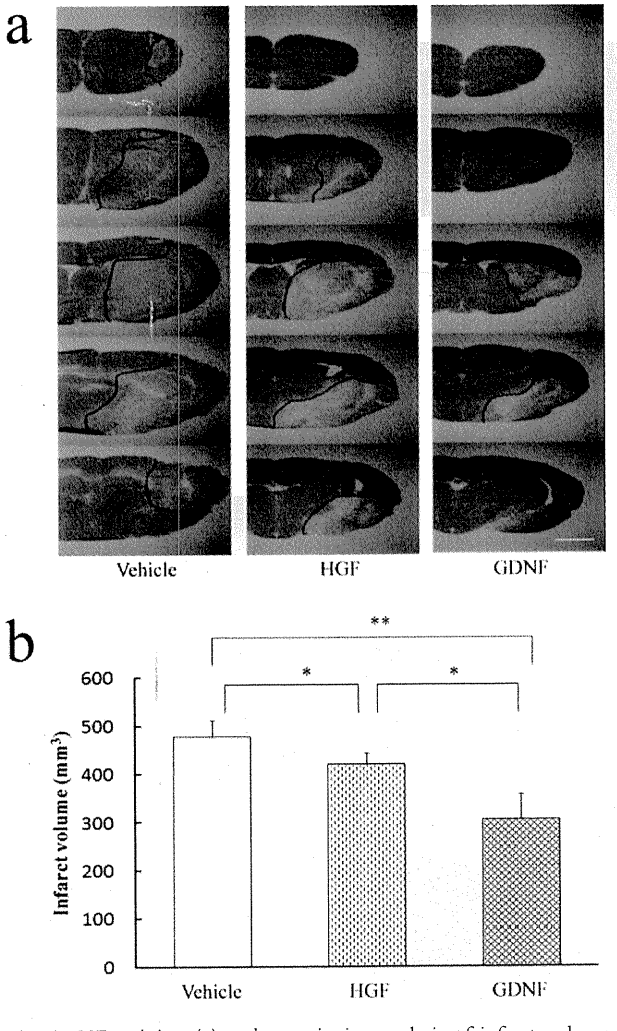

Fig. 1. HE staining (**a**) and quantitative analysis of infarct volume at 24 hr after the reperfusion (**b**). The infarct volume of GDNF (**$P < 0.01$)- and HGF (*$P < 0.05$)-treated groups was significantly smaller than that of vehicle-treated group. Scale bar = 5 mm.

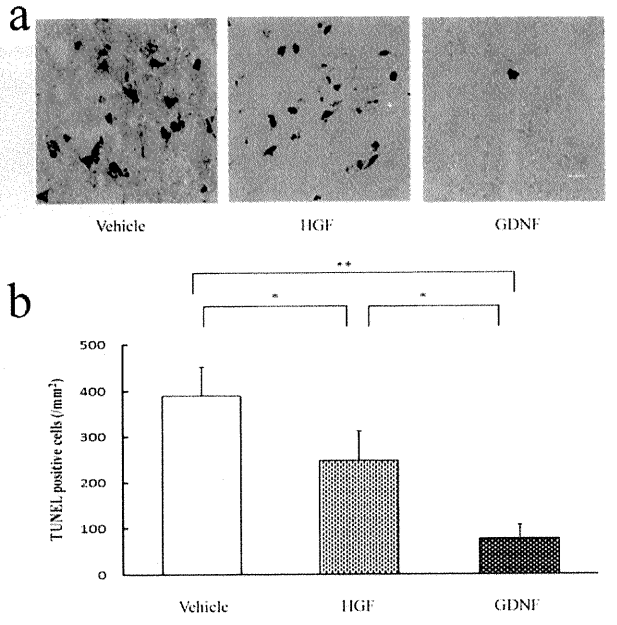

Fig. 2. TUNEL staining (**a**) and quantitative analysis of TUNEL-positive cells for evaluating antiapoptotic effect at 24 hr after reperfusion (**b**). A strong staining for TUNEL was present in the vehicle group, but the treatment with GDNF (**$P < 0.01$) and HGF (*$P < 0.05$) greatly reduced the number of TUNEL-positive cells (*$P < 0.05$). Scale bar = 20 μm.

0.01) and HGF (*$P < 0.05$) greatly reduced the number of TUNEL-positive cells at 24 hr after 90 min of MCAO: 389.8 ± 63.7/mm^2 in vehicle-treated group, 247.5 ± 54.5/mm^2 in HGF-treated group, 76.2 ± 32.1/mm^2 in GDNF-treated group (mean ± SD; Fig. 2a,b).

Antiautophagic Effect

Examining the intracellular localization of LC3 in the ischemic brain. Cerebral ischemia induces autophagy (Adhami et al., 2006; Rami et al., 2008). To show whether the protective effects of GDNF and HGF are associated with the antiautophagic effect after cerebral ischemia, we examined the protein level of LC3 in ischemic and normal brains (Fig. 3a). The number of cells displaying punctate LC3 fluorescence significantly increased after cerebral ischemia, and the numbers in GDNF- and HGF-treated groups significantly decreased compared with the vehicle-treated group ($P < 0.05$; Fig. 3b): 33.5 ± 5.7/mm^2 in sham group, 152.6 ± 23.4/mm^2 in vehicle-treated group, 106.1 ± 15.9/mm^2 in HGF-treated group, 64.7 ± 19.9/mm^2 in GDNF-treated group (mean ± SD). Double-immunofluorescence studies were performed for LC3 and for various brain cell type markers (NeuN to identify neuronal cells, GFAP to identify astrocytes, and NAGO to identify vascular endothelium cells) after cerebral ischemia. Confocal microscopy analysis of the double-stained sections indicated that LC3 and NeuN or GFAP or NAGO were expressed in the same cell (Fig. 3c). Semiquantitative assessment showed that approximately 57% of LC3-positive cells presented both LC3 and NeuN, 30% presented both LC3 and GFAP, and 13% presented both LC3 and NAGO (Fig. 3d).

Western blot analysis for LC3-I and LC3-II in the infarct hemisphere. The amounts of LC3-I plus LC3-II (relative to β-tubulin) were significantly higher in the vehicle-, HGF-, and GDNF-treated groups than in the sham group ($P < 0.05$), and those in the GDNF- and HGF-treated group significantly decreased compared with the vehicle-treated group ($P < 0.05$): 1.39 ± 0.04 in sham group, 3.15 ± 0.30 in vehicle-treated group, 2.64 ± 0.18 in HGF-treated group, 2.13 ± 0.14 in GDNF-treated group (mean ± SD). The amounts of

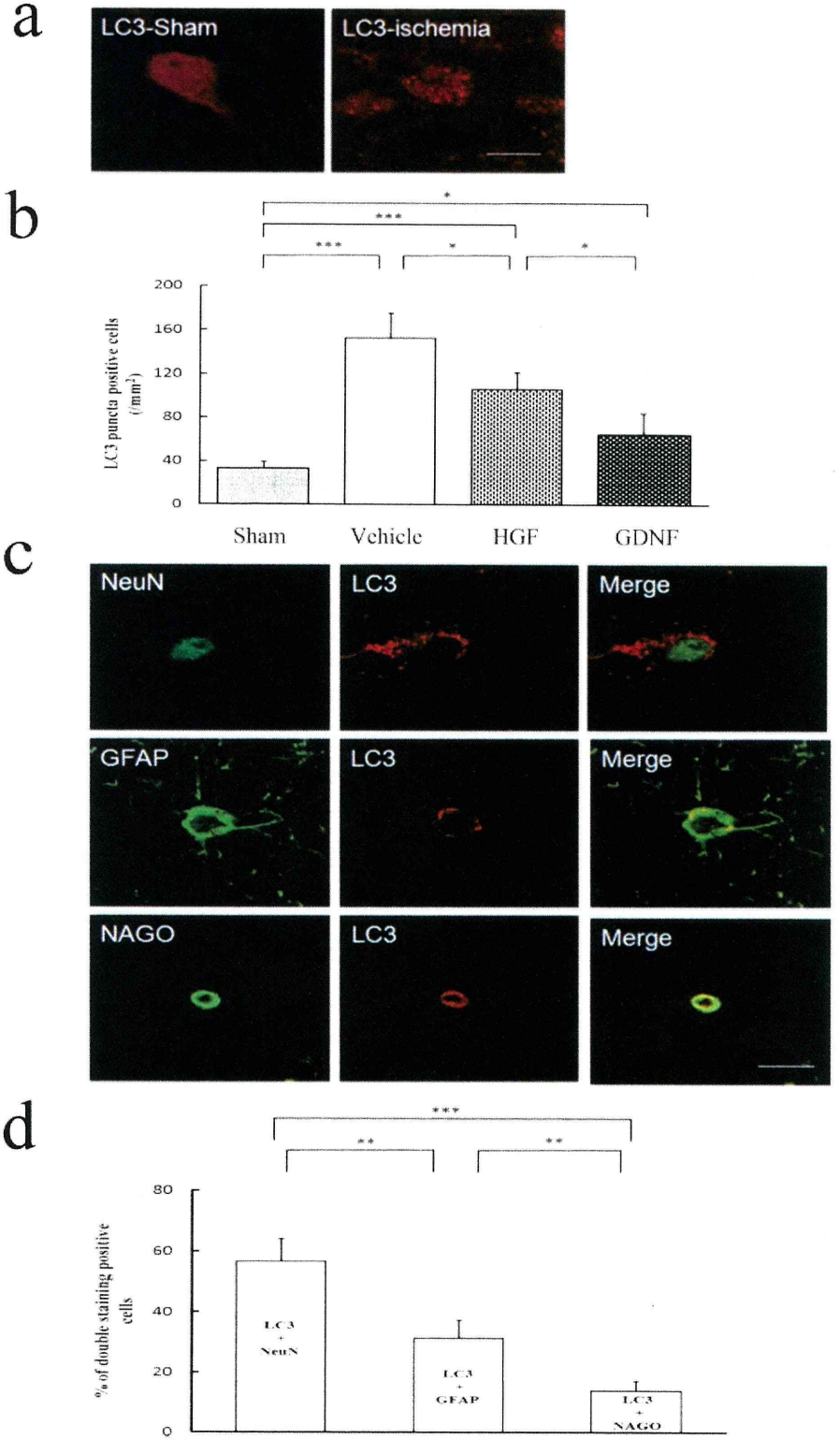

Fig. 3. Immunofluorescence of LC3 in sham and in ischemic brain (**a**) and quantitative analysis of cells with punctate LC3 fluorescence (**b**). Double staining of LC3 and NeuN or GFAP or NAGO in ischemic brain (**c**) and semiquantitative analysis of cells with LC3 and NeuN or GFAP or NAGO fluorescence (**d**). The numbers of cells displaying punctate LC3 fluorescence significantly increased after cerebral ischemia (***$P < 0.001$), and the numbers in the GDNF- and HGF-treated groups significantly decreased compared with the vehicle-treated group (*$P < 0.05$). Although LC3 and NeuN or GFAP or NAGO are expressed in the same cell, LC3 is expressed mainly in neurons in the cerebral cortex and dorsal caudate of the MCA territory. Scale bars = 20 μm in a; 20 μm in c.

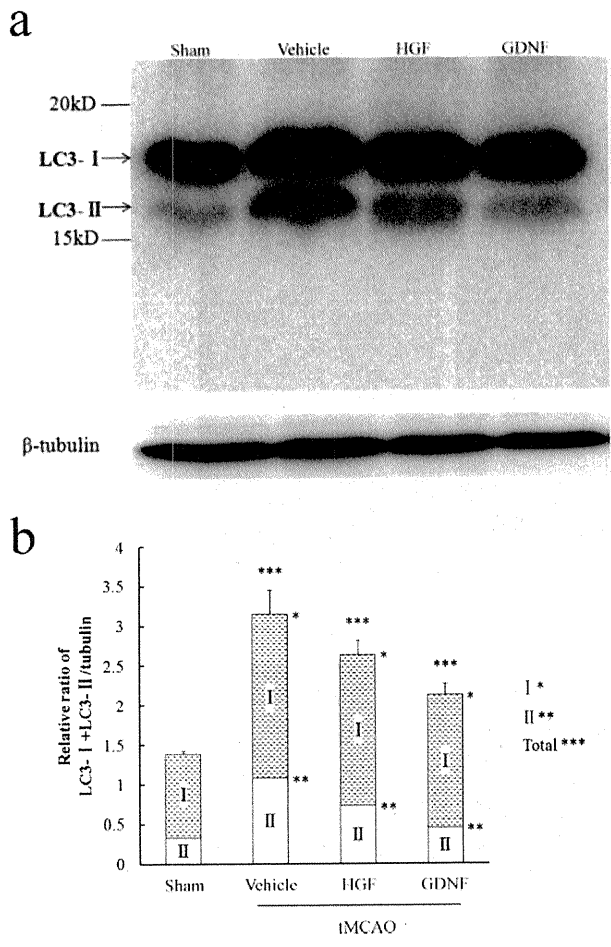

Fig. 4. Western blot analysis of infarct hemisphere for LC3 protein (**a**) and quantitative analysis relative to β-tubulin (**b**). The amounts of LC3-I plus LC3-II and LC3-II (relative to β-tubulin) were significantly higher in the vehicle-, HGF-, and GDNF-treated groups than in the sham group ($P < 0.05$), and those of the GDNF- and HGF-treated group significantly decreased compared with the vehicle-treated group ($P < 0.05$). The amounts of LC3-I (relative to β-tubulin) were significantly higher in the vehicle-, HGF-, and GDNF-treated groups than in the sham group ($P < 0.05$), but there was no difference among them. $*P < 0.05$ for LC3-I vs. sham, $**P < 0.05$ for LC3-II vs. sham, $***P < 0.01$ for LC3-I plus LC3-II vs. sham.

LC3-I were significantly higher in the vehicle-, HGF-, and GDNF-treated groups than in the sham group ($P < 0.05$), but there was no difference among them. The result for LC3-II change was the same as for LC3-I plus LC3-II (Fig. 4a,b).

Single-immunofluorescence analysis of p-mTOR. Immunofluorescence staining of sections with an antibody against p-mTOR showed that the number of immunopositive neurons in the cerebral cortex and dorsal caudate of the MCA territory significantly increased in the HGF ($*P < 0.05$)- and GDNF ($**P < 0.01$)-treated groups: 414.2 ± 78.5/mm^2 in vehicle-

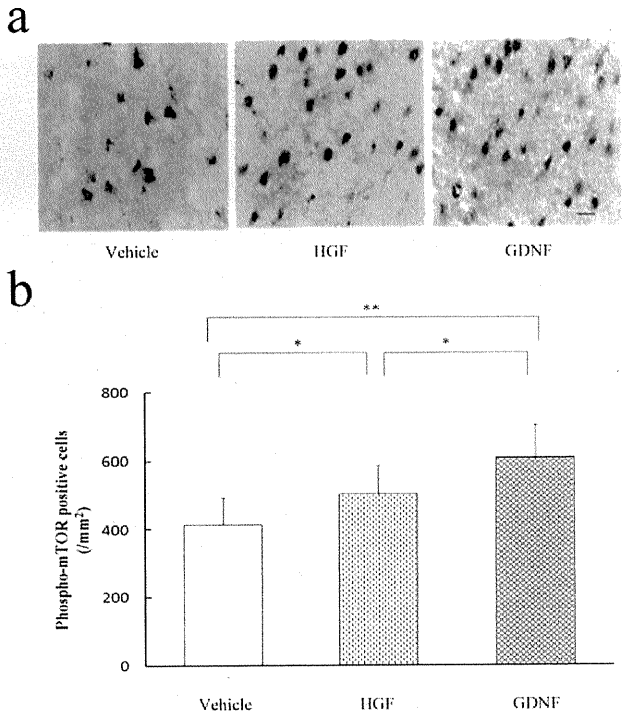

Fig. 5. Immunofluorescence of p-mTOR in the cerebral cortex and dorsal caudate of the MCA territory (**a**) and quantitative analysis of p-mTOR-positive cells (**b**). The number of p-mTOR-positive cells significantly increased in the HGF ($*P < 0.05$)- and GDNF ($**P < 0.01$)-treated groups. Scale bar = 20 μm.

treated group, 502.4 ± 85.2/mm^2 in HGF-treated group, 607.4 ± 96.7/mm^2 in GDNF-treated group (mean ± SD; Fig. 5a,b).

Double-immunofluorescence analysis of LC3/TUNEL staining. Immunofluorescence analysis showed that both LC3 and TUNEL are expressed mainly in neurons in the cerebral cortex and dorsal caudate of the MCA territory. The number of LC3/TUNEL double-positive cells significantly decreased in the HGF ($P < 0.05$)- and GDNF ($P < 0.01$)-treated groups: 238 ± 49.2/mm^2 in vehicle-treated group, 142.8 ± 38.4/mm^2 in HGF-treated group, 71.4 ± 25.2/mm^2 in GDNF-treated group (mean ± SD; Fig. 6a–c).

DISCUSSION

It was reported that GDNF signals via multicomponent receptors consisting of the Ret receptor tyrosine kinase plus a glycosylphosphatidylinositol-linked coreceptor termed *GDNF family receptor* α*1* (GFRα1). After binding to its specific receptor complex, GDNF activates several downstream intracellular pathways, including phosphatidylinositol 3-kinase/protein kinase B (PI3K/Akt; Soler et al., 1999) and extracellular signal-regulated kinase 1/2/mitogen-activated protein kinase (ERK1/2 MAPK) pathways (Worby et al., 1996). Signals through PI3K/Akt or ERK1/2MAPK pathways lead to different

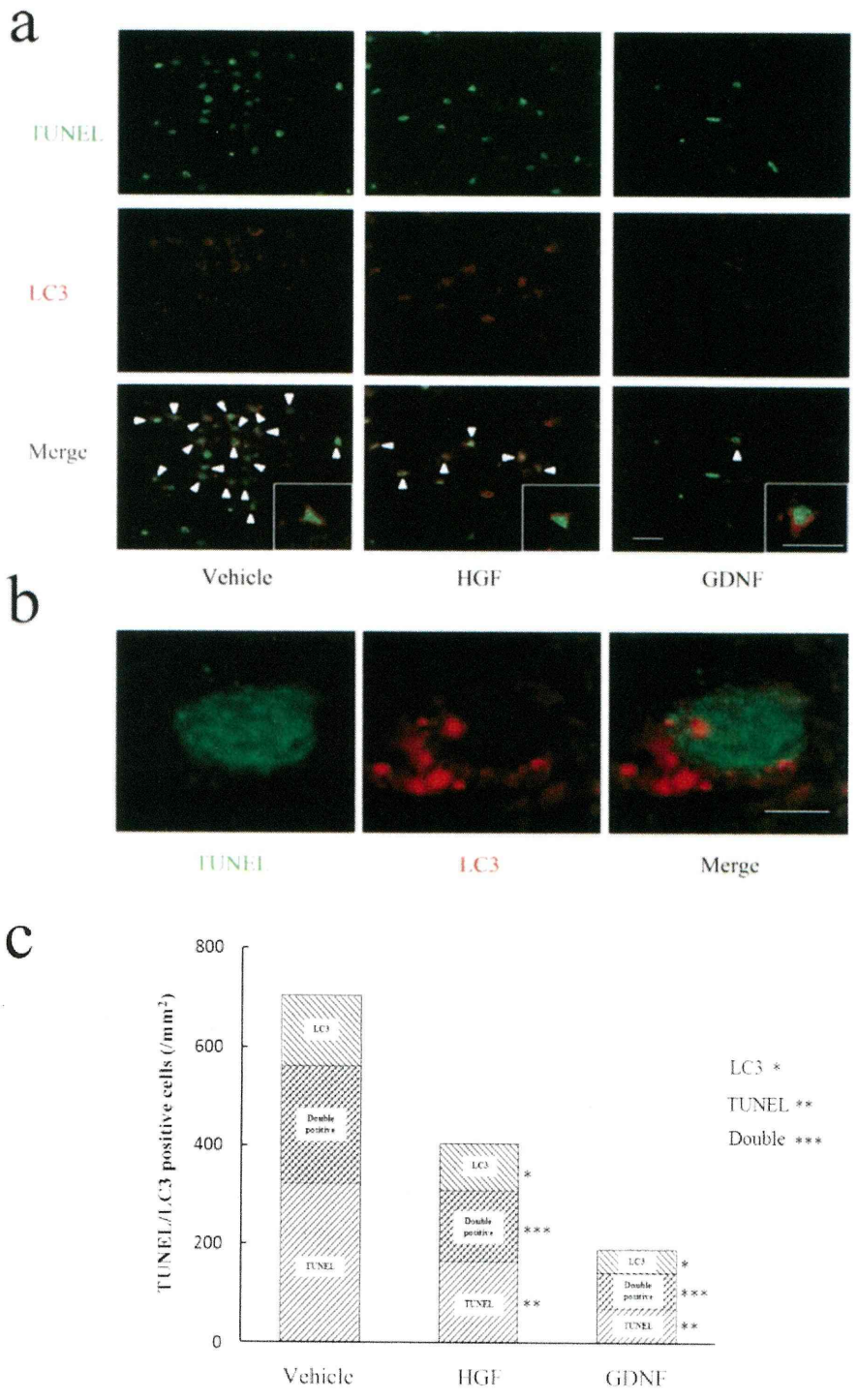

Fig. 6. Photomicrographs of LC3/TUNEL double staining (**a,b**) and quantitative analysis of LC3/TUNEL double-positive cells (**c**). The numbers of LC3/TUNEL double-positive cells significantly decreased in the HGF ($P < 0.05$)- and GDNF ($P < 0.01$)-treated groups. *$P < 0.05$ for LC3 vs. vehicle, **$P < 0.05$ for TUNEL vs. vehicle, ***$P < 0.05$ for double vs. vehicle. Scale bars = 50 μm in a; 20 μm in insets; 10 μm in b.

trophic effects. The most widespread paradigm is that the PI3K/Akt pathway is involved in the cellular survival (Hetman et al., 1999; Vaillant et al., 1999), whereas the ERK1/2 MAPK pathway is involved in neuronal differentiation (Perron et al., 1999). HGF activates the protooncogenic receptor tyrosine kinase c-MET and subsequent downstream pathways, including the antiapoptotic protein kinase-B (PKB/Akt) cascade, the proliferative MAP-kinase pathway (ERK1/2 and p38MAPK), and the STAT3 signaling (signal transducers and activators of transcription; Birchmeier et al., 2003; Okano et al., 2003; Hanada et al., 2004). Similarly, activation of the PI3 kinase/Akt pathway, which is a well known way to inhibit apoptosis, also inhibits autophagy (Arico et al., 2001). Thus, perhaps GDNF and HGF significantly reduced infarct size associated with both the antiapoptotic and the antiautophagic effects (Fig. 1).

From the results of TUNEL staining (Fig. 2), GDNF and HGF had significant antiapoptotic effects. Autophagy was first described in the 1960s (Stromhaug and Klionsky, 2001; Kundu and Thompson, 2008), but many questions about the actual processes and mechanisms involved remain to be elucidated. In multicellular organisms, autophagy is a homeostatic mechanism that may represent the first stage in a cellular/tissue response that can range from autophagy to apoptosis and necrosis (Klionsky and Emr, 2000). In this sense, autophagy is a protective mechanism that can eliminate cells that would otherwise prove harmful to the organism. In fact, autophagy has been suggested to play a critical role in type II (nonapoptotic) programmed cell death (Klionsky and Emr, 2000). To show whether the protective effects of GDNF and HGF are associated with the antiautophagic effect after cerebral ischemia, we examined the protein level of LC3 in ischemic and normal brains. LC3 is associated with autophagosome membranes after post-translational modifications. A C-terminal fragment of LC3 is cleaved immediately after synthesis to yield a cytosolic form called *LC3-I* (18 kDa). A subpopulation of LC3-I is further converted to an autophagosome-associating form, LC3-II (16 kDa). It was reported that the amount of LC3-II was correlated with the extent of autophagosome formation (Kabeya et al., 2000, 2004). The conversion of LC3-I into LC3-II is accepted as a simple method for monitoring autophagy (Mizushima, 2004; Klionsky et al., 2007). We probed brain sections with an LC3 antibody that detects both forms of LC3, and strong LC3-immunopositive puncta were observed in ischemic brains (Fig. 3a,b). LC3 can under some conditions be incorporated into protein aggregates (Kuma et al., 2007). This is in accordance with Rami et al. (2008), and we found that LC3 is expressed mainly in neurons in the cerebral cortex and dorsal caudate of the MCA territory (Fig. 3c,d).

Western blot analysis of LC3 was performed in our study as well, and we detected that the amount of LC3-I plus LC3-II was significantly higher after cerebral ischemia and that the amount of LC3-II change was crucial in that (Fig. 4). The number of LC3-positive cells or the amount of LC3 was significantly decreased with GDNF and HGF treatments.

Mammalian target of rapamycin (mTOR) is a phosphatidyl inositol kinase-related kinase that negatively regulates autophagy (Schmelzle and Hall, 2000; Yorimitsu and Klionsky, 2005). It has been reported that mTOR function is activated by phosphorylation of Ser^{2448} (Nave et al., 1999; Ravikumar et al., 2003). Recent studies have presented evidence that insulin signal stimulates phosphorylation and activity of mTOR via Akt/PKB signaling (Schmelzle and Hall, 2000). In our study, we confirmed that the level of p-mTOR, an activated form, increased in the HGF and GDNF treated groups (Fig. 5). It can also be hypothesized that GDNF and HGF partially regulated autophagy by the mTOR intracellular signaling pathway. The results described above suggested that both GDNF and HGF have significant antiautophagic effects. Our study suggests that the protective effects of GDNF and HGF were greatly associated both with antiapoptotic and with antiautophagic effects in terms of reducing the number of TUNEL-positive cells, LC3, and activating mTOR. The number of LC3/TUNEL double-positive cells was about 34.3% of LC3 plus TUNEL-positive cells after cerebral ischemia (Fig. 6), which suggested that perhaps one cell can undergo apoptotic cell death or autophagic cell death or two types of cell death at the same time. Thus, it is possible that there are relations between apoptosis and autophagy. It was reported that apoptosis regulator also interacts physically with an autophagy regulator; for example, Beclin 1 can prevent autophagy induction. Beclin 1 was identified as a Bcl-2 interacting protein (Liang et al., 1999), and Beclin 1 also interacts with the other major antiapoptotic Bcl family protein (Bcl-xL) and increases autophagy in nutrient-deprived or growth-factor-withdrawn cells, allowing cell survival (Boya et al., 2005; Lum et al., 2005) by inhibiting apoptosis. In this regard, perhaps in the future GDNF and HGF will be used in cerebral ischemia to protect against neuronal damage. We propose that both GDNF and HGF could provide important therapeutic benefits in terms of not only antiapoptotic but also antiautophagic effects for acute stroke patients. However, when gelfoam is chosen for the delivery of these factors, the amounts of GDNF and HGF should be carefully redetermined before clinical use of these proteins, because better neuroprotective effects in cerebral ischemia have been proved when these proteins are applied intrastriatally or intraventricluarly using an osmotic pump (Miyazawa et al., 1998; Tsuzuki et al., 2000). Differential roles of GDNF and HGF in chronic cerebral ischemia are of great interests and are bcurrently under investigation in terms of the presence of various extraneurotrophic activities of HGF (Funakoshi and Nakamura, 2003).

ACKNOWLEDGMENTS

We thank Kringle Pharma (Osaka, Japan) for the gift of HGF. The authors declare that they have no competing financial interests.

REFERENCES

Abe K, Kawagoe J, Araki T, Aoki M, Kogure K. 1992. Differential expression of heat shock protein 70 gene between the cortex and caudate after transient focal cerebral ischemia in rats. Neurol Res 14:381–385.

Abe K, Hayashi T, Itoyama Y. 1997. Amelioration of brain edema by topical application of glial cell line-derived neurotrophic factor in reperfused rat brain. Neurosci Lett 231:37–40.

Adhami F, Liao G, Morozov YM, Schloemer A, Schmithorst VJ, Lorenz JN, Dunn RS, Vorhees CV, Wills-Karp M, Degen JL, Davis RJ, Mizushima N, Rakic P, Dardzinski BJ, Holland SK, Sharp FR, Kuan CY. 2006. Cerebral ischemia-hypoxia induces intravascular coagulation and autophagy. Am J Pathol 169:566–583.

Arico S, Petiot A, Bauvy C. 2001. The tumor suppressor PTEN positively regulates macroautophagy by inhibiting the phosphatidylinositol 3-kinase/protein kinase B pathway. J Biol Chem 276:35243–35246.

Augustin HG, Braun K, Telemenakis I, Modlich U, Kuhn W. 1995. Ovarian angiogenesis. Phenotypic characterization of endothelial cells in a physiological model of blood vessel growth and regression. Am J Pathol 147:339–351.

Beck KD, Valverde J, Alexi T, Poulsen K, Moffat B, Vandlen RA, Rosenthal A, Hefti F. 1995. Mesencephalic dopaminergic neurons protected by GDNF from axotomy-induced degeneration in the adult brain. Nature 373:339–341.

Birchmeier C, Birchmeier W, Gherardi E, Vande Woude GF. 2003. Met, metastasis, motility and more. Nat Rev Mol Cell Biol 4:915–925.

Bottaro DP, Rubin JS, Faletto DL, Chan AM, Kmiecik TE, Vande Woude GF, Aaronson SA. 1991. Identification of the hepatocyte growth factor receptor as the c-Met proto-oncogene product. Science 251:802–804.

Boya P, Gonzalez-Polo RA, Casares N. 2005. Inhibition of macroautophagy triggers apoptosis. Mol Cell Biol 25:1025–1040.

Cotran RS, Kumar V, Collins T. 1998. Cell injury and cellular death. In: Cotran RS, Kumar V, Collins T, editors. Robbins pathologic basis of disease,6th ed. Philadelphia: Lippincott. p1–29.

Feig C, Peter ME. 2007. How apoptosis got the immune system in shape. Eur J Immunol 37(Suppl 1):S61–S70.

Funakoshi H, Nakamura T. 2003. Hepatocyte growth factor: from diagnosis to clinical applications. Clin Chim Acta 327:1–23.

Galluzzi L. 2007. Cell death modalities: classification and pathophysiological implications. Cell Death Differ 14:1237–1243.

Green D, Kroemer G. 1998. The central executioner of apoptosis: mitochondria or caspases? Trends Cell Biol 8:267–271.

Hanada M, Feng J, Hemmings BA. 2004. Structure, regulation and function of PKB/AKT—a major therapeutic target. Biochim Biophys Acta 1697:3–16.

Henderson CE, Phillips HS, Pollock RA, Davies AM, Lemeulle C, Armanini M, Simpson LC, Moffet B, Vandlen RA, Koliatsos VE, Rosenthal A. 1997. GDNF: a potent survival factor for motoneurons present in peripheral nerve and muscle. Science 266:1062–1064.

Hetman M, Kanning K, Cavanaugh JE, Xia ZG. 1999. Neuroprotection by brainderived neurotrophic factor is mediated by extracellular signal-regulated kinase and phosphatidylinositol 3-kinase. J Biol Chem 274:22569–22580.

Honda S, Kagoshima M, Wanaka A, Tohyama M, Matsumoto K, Nakamura T. 1995. Localization and functional coupling of HGF and c-Met/HGF receptor in rat brain: implication as neurotrophic factor. Brain Res Mol Brain Res 32:197–210.

Inbal B, Bialik S, Sabanay I, Shani G, Kimchi A. 2002. DAP kinase and DRP-1 mediate membrane blebbing and the formation of autophagic vesicles during programmed cell death. J Cell Biol 157:455–468.

Kabeya Y, Mizushima N, Ueno T, Yamamoto A, Kirisako T, Noda T, Kominami E, Ohsumi Y, Yoshimori T. 2000. LC3, a mammalian homologue of yeast Apg8p, is localized in autophagosome membranes after processing. EMBO J 19:5720–5728.

Kabeya Y, Mizushima N, Yamamoto A, Oshitani-Okamoto S, Ohsumi Y, Yoshimori T. 2004. LC3, GABARAP and GATE16 localize to autophagosomal membrane depending on form-II formation. J Cell Sci 117:2805–2812.

Kerr JF, Wyllie AH, Currie AR. 1972. Apoptosis: a basic biological phenomenon with wide-ranging implications in tissue kinetics. Br J Cancer 26:239–257.

Kirisako T, Baba M, Ishihara N, Miyazawa K, Ohsumi M, Yoshimori T, Noda T, Ohsumi Y. 1999. Formation process of autophagosome is traced with Apg8/Aut7p in yeast. J Cell Biol 147:435–446.

Kitagawa H, Hayashi T, Mitsumoto Y, Koga N, Itoyama Y, Abe K. 1998. Reduction of ischemic brain injury by topical application of glial cell line-derived neurotrophic factor after permanent middle cerebral artery occlusion in rats. Stroke 29:1417–1422.

Klionsky DJ, Emr SD. 2000. Autophagy as a regulated pathway of cellular degradation. Science 290:1717–1721.

Klionsky DJ, Cregg JM, Dunn WA, Emr SD, Sakai Y, Sandoval IV, Sibirny S, Subramani S, Thumm M, Veenhuis M, Ohsumi Y. 2003. A unified nomenclature for yeast autophagy-related genes. Dev Cell 5: 539–545.

Klionsky DJ, Cuervo AM, Seglen PO. 2007. Methods for monitoring autophagy from yeast to human. Autophagy 3:181–206.

Koizumi J, Yoshida Y, Nakazawa T, Ooneda G. 1986. Experimental studies of ischemic brain edema: A new experimental model of cerebral embolism in rats in which recirculation can be induced in the ischemic area. Jpn J Stroke 8:1–7.

Kroemer G. 2005. Classification of cell death: recommendations of the Nomenclature Committee on Cell Death. Cell Death Differ 12(Suppl 2):1463–1467.

Kuma A, Matsui M, Mizushima N. 2007. LC3, an autophagosome marker, can be incorporated into protein aggregates independent of autophagy. Autophagy 3:328–332.

Kundu M, Thompson CB. 2008. Autophagy: basic principles and relevance to disease. Annu Rev Pathol 3:427–455.

Liang XH, Jackson S, Seaman M. 1999. Induction of autophagy and inhibition of tumorigenesis by beclin 1. Nature 402:672–676.

Lin L-FH, Doherty DH, Lile JD, Bektesh S, Collins F. 1993. GDNF: a glial cell line-derived neurotrophic factor for midbrain dopaminergic neurons. Science 260:1130–1132.

Lin L, Wu W, Lin LF, Lei M, Oppenheim RW, Houenou LJ. 1995. Rescue of adult mouse motoneurons from injury-induced cell death by glial cell line-derived neurotrophic factor. Proc Natl Acad Sci U S A 92:9771–9775.

Lum JJ, Bauer DE, Kong M. 2005. Growth factor regulation of autophagy and cell survival in the absence of apoptosis. Cell 120:237–248.

Maina F, Klein R. 1999. Hepatocyte growth factor, a versatile signal for developing neurons. Nat Neurosci 2:213–217.

Maina F, Hilton MC, Andres R, Wyatt S, Klein R, Davies AM. 1998. Multiple roles for hepatocyte growth factor in sympathetic neuron development. Neuron 20:835–846.

Matsumoto K, Nakamura T. 1996. Emerging multipotent aspects of hepatocyte growth factor. J Biochem 119:591–600.

Matsumoto K, Nakamura T. 1997. Hepatocyte growth factor (HGF) as a tissue organizer for organogenesis and regeneration. Biochem Biophys Res Commun 239:639–644.

Miyazawa T, Matsumoto K, Ohmichi H, Katoh H, Yamashima T, Nakamura T. 1998. Protection of hippocampal neurons from ischemia-induced delayed neuronal death by hepatocyte growth factor: a novel neurotrophic factor. J Cereb Blood Flow Metab 18:345–348.

Mizushima N. 2004. Methods for monitoring autophagy. Int J Biochem Cell Biol 36:2491–2502.

Nagasawa H, Kogure K. 1989. Correlation between cerebral blood flow and histologic changes in a new rat model of middle cerebral artery occlusion. Stroke 20:1037–1043.

Nakamura T, Nawa K, Ichihara A. 1984. Partial purification and characterization of hepatocyte growth factor from serum of hepatectomized rats. Biochem Biophys Res Commun 122:1450–1459.

Nakamura T, Nishizawa T, Hagiya M, Seki T, Shimonishi M, Sugimura A, Tashiro K, Shimizu S. 1989. Molecular cloning and expression of human hepatocyte growth factor. Nature 342:440–443.

Nave BT, Ouwens M, Withers DJ, Alessi DR, Shepherd PR. 1999. Mammalian target of rapamycin is a direct target for protein kinase B: identification of a convergence point for opposing effects of insulin and amino-acid deficiency on protein translation. Biochem J 344:427–431.

Niimura M, Takagi N, Takagi K, Funakoshi H, Nakamura T, Takeo S. 2006a. Effects of hepatocyte growth factor on phosphorylation of extracellular signal-regulated kinase and hippocampal cell death in rats with transient forebrain ischemia. Eur J Pharmacol 27:114–124.

Niimura M, Takagi N, Takagi K, Mizutani R, Ishihara N, Matsumoto K, Funakoshi H, Nakamura T, Takeo S. 2006b. Prevention of apoptosis-inducing factor translocation is a possible mechanism for protective effects of hepatocyte growth factor against neuronal cell death in the hippocampus after transient forebrain ischemia. J Cereb Blood Flow Metab 26:1354–1365.

Okano J, Shiota G, Matsumoto K, Yasui S, Kurimasa A, Hisatome I, Steinberg P, Murawaki Y. 2003. Hepatocyte growth factor exerts a proliferative effect on oval cells through the PI3K/AKT signaling pathway. Biochem Biophys Res Commun 309:298–304.

Otto D, Frotscher M, Unisicker K. 1989. Basic fibroblast growth factor and nerve growth factor administrated in gel foam rescue medial septal neurons after fimbria fornix transection. J Neurosci Res 22:83–91.

Perron JC, Bixby JL. 1999. Distinct neurite outgrowth signaling pathways converge on ERK activation. Mol Cell Neurosci 13:362–378.

Rami A, Langhagen A, Steiger S. 2008. Focal cerebral ischemia induces up-regulation of Beclin 1 and autophagy-like cell death. Neurobiol Dis 29:132–141.

Ravikumar B, Stewart A, Kita H, Kato K, Duden R, Rubinsztein DC. 2003. Raised intracellular glucose concentrations reduce aggregation and cell death caused by mutant huntingtin exon 1 by decreasing mTOR phosphorylation and inducing autophagy. Hum Mol Genet 12:985–994.

Reggiori F, Klionsky DJ. 2002. Autophagy in the eukaryotic cell. Eukaryot. Cell 1:11–21.

Russell WE, McGowan JA, Bucher NL. 1984. Partial characterization of a hepatocyte growth factor from rat platelets. J Cell Physiol 119:183–192.

Schmelzle T, Hall MN. 2000. TOR, a central controller of cell growth. Cell 103:253–262.

Soler RM, Dolcet X, Encinas M, Egea J, Bayascas JR, Comella JX. 1999. Receptors of the glial cell line-derived neurotrophic factor family of neurotrophic factors signal cell survival through the phosphatidylinositol 3-kinase pathway in spinal cord motoneurons. J Neurosci 19: 9160–9169.

Stromhaug PE, Klionsky DJ. 2001. Approaching the molecular mechanism of autophagy. Traffic 2:524–531.

Sun W, Funakoshi H, Nakamura T. 2002. Overexpression of HGF retards disease progression and prolongs life span in a transgenic mouse model of ALS. J Neurosci 22:6537–6548.

Tomac A, Lindqvist E, Lin LF, Gren SO, Young D, Hoffer BJ, Olson L. 1995. Protection and repair of the nigrostriatal dopaminergic system by GDNF in vivo. Nature 373:335–339.

Tsuzuki N, Miyazawa T, Matsumoto K, Nakamura T, Shima K, Chigasaki H. 2000. Hepatocyte growth factor reduces infarct volume after transient focal cerebral ischemia in rats. Acta Neurochir Suppl 76:311–316.

Tsuzuki N, Miyazawa T, Matsumoto K, Nakamura T, Shima K. 2001. Hepatocyte growth factor reduces the infarct volume after transient focal cerebral ischemia in rats. Neurol Res 23:417–424.

Vaillant AR, Mazzoni I, Tudan C, Boudreau M, Kaplan DR, Miller FD. 1999. Depolarization and neurotrophins converge on the phosphatidylinositol 3-kinase-Akt pathway to synergistically regulate neuronal survival. J Cell Biol 146:955–966.

Van Belle E, Witzenbichler B, Chen D, Silver M, Chang L, Schwall R, Isner JM. 1998. Potentiated angiogenic effect of scatter factor/hepatocyte growth factor via induction of vascular endothelial growth factor: the case for paracrine amplification of angiogenesis. Circulation 97:381–390.

Wang Y, Lin SZ, Chiou AL, Williams LR, Hoffer BJ. 1997. Glial cell line-derived neurotrophic factor protects against ischemia-induced injury in the cerebral cortex. J Neurosci 17:4341–4348.

Worby CA, Vega QC, Zhao Y, Chao HH, Seasholtz AF, Dixon JE. 1996. Glial cell line-derived neurotrophic factor signals through the RET receptor and activates mitogen-activated protein kinase. J Biol Chem 271:23619–23622.

Yorimitsu T, Klionsky DJ. 2005. Autophagy: molecularmachinery for self-eating. Cell Death Differ 12(Suppl 2):1542–1552.

Yoshimori T. 2004. Autophagy: a regulated bulk degradation process inside cells. Biochem Biophys Res Commun 313:453–458.

Zarnegar R, Michalopoulos GK. 1995. The many faces of hepatocyte growth factor: from hepatopoiesis to hematopoiesis. J Cell Biol 129:1177–1180.

Zhao MZ, Nonoguchi N, Ikeda N, Watanabe T, Furutama D, Miyazawa D, Funakoshi H, Kajimoto Y, Nakamura T, Dezawa M, Shibata MA, Otsuki Y, Coffin RS, Liu WD, Kuroiwa T, Miyatake S. 2006. Novel therapeutic strategy for stroke in rats by bone marrow stromal cells and ex vivo HGF gene transfer with HSV-1 vector. J Cereb Blood Flow Metab 26:1176–1188.